



Mineral chemistry (EMPA) of monazites in metamorphic rocks from Edea region: implications of the monazite chemistry on the metamorphic evolution of the Nyong Complex

Ndema Mbongué Jean Lavenir^{1,2} · Sigué Cyrille^{1,2} · Nzenti Jean Paul² · Cheo Emmanuel Suh¹

Received: 26 April 2022 / Accepted: 13 October 2022 / Published online: 5 November 2022
© Saudi Society for Geosciences 2022

Abstract

The Edea region is situated in the Nyong Complex within the Northwestern edge of the Congo craton in Cameroon. The back scattered electron image and the mineral composition of monazite were determined using an electron microprobe analytical technique. The objective of this study was to constraint the geochemical and the textural composition on the behavior of metamorphic monazites on the EMP in issue to delineate the metamorphic evolution of the Nyong Complex. Metamorphic Th-rich monazite-(Ce) exhibiting a predominance of LREEs, with Ce as dominant REEs, were recorded in meta-igneous rocks and metasedimentary rocks. Irrespective of core and rim domains, monazite of sample ED4B and M4 have 85 to 98 mol% monazite content and characterized by low cheralite content (< 7 mol%). Monazite from sample ED3D yields huttonitic monazite (45–75 mol% monazite content) and monazite (75–98 mol%) fields; they are characterized by low cheralite (< 5 mol%), high monazite (75–98 mol%), relative high cheralite (6–12 mol%), and low monazite (65–80 mol%). Monazite compositions are linked by dominantly huttonitic and cheralite substitutions. The metamorphic evolution indicates that both meta-igneous rocks and metasedimentary rocks of the Nyong Complex are overprinted by two respective high-grade phases of metamorphism. The first phase of metamorphism in the meta-igneous rocks is underlined by globular monazite grains; the second phase is characterized by elongated and oriented monazite crystals following the mylonitic foliation S_1 . The first phase of metamorphism in metasedimentary rocks is marked by ovoid grains of monazite; the last phase is characterized by elongated and oriented monazites which mimic the S_2 schistosity.

Keywords Edea region · Nyong Complex · Th-rich monazite-(Ce) · Mylonitic foliation S_1 · Huttonitic monazite · Huttonitic and cheralite substitutions

Introduction

The phosphate mineral monazite (LREE,Th,Y,Si,Ca)PO₄ was first reported as an igneous accessory phase in peraluminous granites, syenite, and granitic pegmatites, quartz veins, and carbonatites (Breithaupt 1829). It also occurs as an accessory mineral in metapelites with Ca-poor and Al-rich bulk compositions at all metamorphic grades above the upper greenschist facies. This mineral occurs in low-pressure contact metamorphic rocks; in high-grade garnet cordierite K-feldspar gneisses; in granulites, migmatites, and charnockites; and in coesite-bearing ultra-high-pressure garnet gneisses (Overstreet 1967; Spear and Pyle 2002; Brandt et al. 2011; Petrík et al. 2019). Monazite is not an approved high-pressure phase and apparently crystallizes prior to and/or after to the peak pressures. It is also observed in connection

Responsible Editor: Domenico M. Doronzo

✉ Ndema Mbongué Jean Lavenir
jndema2012@gmail.com; ndema.mbongue@ubuea.cm

Sigüé Cyrille
siguecyrille@gmail.com

Nzenti Jean Paul
jnzeni2010@gmail.com

Cheo Emmanuel Suh
chuhma@yahoo.com

¹ Department of Geology, Faculty of Sciences, University of Buea, P.O. Box 63, Buea, Cameroon

² Department of Earth Sciences, Faculty of Sciences, University of Yaoundé I, P.O. Box 812, Yaoundé, Cameroon

with hydrothermal and metasomatic ore deposits (Poitrasson et al. 1996; Seydoux-Guillaume et al. 2012).

Monazite has variable mineral chemical compositions. Its nominal composition is dominated by La, Ce, and Nd which together comprise 2.8–3.2 cations per 4 oxygen of the total cation proportions. The other REE (Pr, Sm, Eu, and Gd) occur in minor proportions (0.3–0.4 a.p.f.u). Because of a lack of great differences between the three different minerals that consist of monazite, these three minerals refer to as one mineral named monazite. The three minerals have differences in their chemical percentages, and these differences are reflected in their respective names. The three monazite types include monazite-(Ce) with the chemical composition (Ce,La,Nd,Th,Y)PO₄; monazite-(La) has (La,Ce,Nd)PO₄ as chemical formula, and monazite-(Nd) which has (Nd,La,Ce)PO₄ as chemical formula. The differences in the formula represent the greater percentages of certain elements in the mineral. For example, monazite-(La) is greatly enriched in lanthanum; monazite-(Ce) consists of Ce-enrichment; it represents the element with the greater percentage in the mineral, and refers to the most common of the three monazites. Furthermore, monazite is the name of a group of monoclinic phosphate and arsenate minerals that share traits of composition and crystal structure (Hobart 2018). A list of minerals in the monazite group is presented in Table 1.

According to Linthout (2007), the nomenclature for the system 2REEPO₄–CaTh(PO₄)₂–2ThSiO₄ has been revised, to be consistent with the Commission on New Minerals and Mineral Names (CNMMN) principles; and only three names are applied to members represented by the respective end-member compositions: monazite, cheralite, and huttonite. The name cheralite with chemical composition (Ce,Ca,Th)·(P,Si)O₄ has priority over brabantite, CaTh(PO₄)₂ which is discredited.

Monazite plays an important role in determining the rare-earth element (REE) contents of the rocks, especially those that are high in silica. It is a monoclinic Ce-phosphate mineral with the ideal formula CePO₄, where Ce can be replaced by the other light rare earth elements (LREE) in any proportion. The co-ordination number for REE is 9, which

is the site in the lattice favored by LREE with bigger ionic radii. Generally, a few percent of La-Sm, Gd, and some tenth of a percent of Eu and heavier REE (less than 0.02 a.p.f.u) including Y (up to 0.1 a.p.f.u) are present (Franz et al. 1996; Heinrich et al. 1997; Förster 1998; Zhu and O’Nions 1999; Spear and Pyle 2002; Linthout 2007). The proportions of the individual REE can differ depending on the conditions of formation. Also, monazite often contains a few percent ThO₂ (up to 20 wt%), less U (up to 2 wt%), Ca, and some Si. The Th occurs in igneous and metamorphic monazite with up to 0.25 a.p.f.u, but most metamorphic monazite has less than 0.05 Th a.p.f.u. Uranium and calcium balance the charge differences of the REE and actinides according to the following reactions: 2REE³⁺ = (Th,U)⁴⁺ + Ca²⁺ or REE³⁺ + P⁵⁺ = (Th,U)⁴⁺ + Si⁴⁺.

Chemically related minerals are (1) xenotime, YPO₄, tetragonal, with a REE co-ordination number of 8, so that it prefers the HREE with smaller ionic radii; (2) cheralite, (Ce,Ca,Th)·(P,Si)O₄, is a member of the monazite CePO₄-brabantite CaTh(PO₄)₂ series, isostructural with monazite (Hughes et al. 1995); (3) rhabdophane, CePO₄·H₂O, or nH₂O, hexagonal; (4) brockite, (Ce,Th,Ca)PO₄·H₂O or nH₂O, hexagonal, a member of the rhabdophane group.

It is well known that monazite grains are formed by various geochemical processes including crystallization, metamorphic reactions, and hydrothermal interactions. In many instances, it is noted that metamorphic monazite overgrows preexisting cores of possible igneous origin. This can be differentiated based on monazite textural occurrence, zoning patterns, and mineral chemistry (Montel et al. 2000; Williams and Jercinovic 2002; Foster and Parrish 2003; Pyle and Spear 2003; Dahl et al. 2005). The great density (4.6–5.7) of monazite makes easy for the crystals to be collected into placer deposits. Monazite is a primary ore of many rare earth metals such as thorium, cerium, and lanthanum. These metals are considered quite valuable and have various industrial uses. For example, thorium is a highly radioactive metal and could be used as a replacement for uranium in nuclear power generation.

In addition to LREE, natural monazites can integrate high quantities of thorium and small percentage of uranium (Parrish 1990). They can also integrate calcium and silicon; it is because of the intervention of these cations that uranium and thorium can integrate the lattice by substitutions (Gardes 2006): huttonite, from the name of the mineral huttonite (ThSiO₄) refers to the first substitution, and brabantite, from the name of the mineral brabantite (Ca_{0.5}Th_{0.5}PO₄), refers to the second substitution. These two minerals form continuous solid-solutions with LREE(PO₄) end-member (Peiffert and Cuney 1999; Montel et al. 2002) and have a monazite structure. Natural monazites vary in composition between these three end-members, and monazite is assumed to contain very

Table 1 List of monazite mineral group (Hobart 2018)

Mineral	Chemical composition
Brabantite	CaTh(PO ₄) ₂
Cheralite	(Ca, Ce,Th)(P,Si)O ₄
Gasparite-(Ce)	(Ce,La,Nd)AsO ₄
Monazite-(Ce)	CePO ₄
Monazite-(La)	LaPO ₄
Monazite-(Nd)	NdPO ₄
Monazite-(Sm)	SmPO ₄
Roseveltite	BiAsO ₄

little (negligible) or no initial Pb (Parrish 1990). Therefore, it is suitable for dating with EMPA. In other words, if Mnz contain initial Pb, it has to be corrected for initial Pb, which is not possible with electron probe microanalyzer (EMPA). Therefore, the mineral chemical and crystallographic characteristics of monazite made it a perfect target for in situ geochronology besides the classical U–Pb isotope measurements by TIMS, SIMS, and LA-MC-ICP-MS (Harrison et al. 2002).

Metamorphic rocks of the Nyong Complex at the western end of Congo Craton contain accessory minerals such as rutile, epidote, and monazites. The aim of this work is to constraint the mineral chemistry of monazite which is the most widespread accessory REE-minerals in Edea region situated in the Nyong Complex. In this purpose, a methodology, implementing the analysis by electron microprobe analysis (EMPA), was used. The significance and the implication in studying the mineral chemistry of monazite of the metamorphic rocks of the Edea area is to delineate the tectono-metamorphic events for better understanding of the metamorphic/deformation history of the Nyong Complex. In the present study, the metamorphic monazite is easily and efficiently localized and mapped using the back scattered electron (BSE) feature on an electron microprobe. On the basis of textural relationships, this allows to delineate the tectono-metamorphic events of the Nyong Complex during the high- grade metamorphism and subsequent temperature, pressure, and age estimation.

Geological setting

Regional geology

In South Cameroon, the Precambrian basement includes three main geotectonic units: the North Equatorial Fold Belt or Oubanguide complexes (Owona et al. 2011) in the north represented by the Yaoundé Group (Nzenti et al. 1988; Ngnotué et al. 2012) and the Ntem and Nyong Complexes in the south which is the northwestern border of the Congo craton (Toteu et al. 1994; Shang et al. 2004, 2010; Tchameni et al. 2004; Pouclet et al. 2007; Owona et al. 2021a; Soh Tamehe et al. 2022; Fig. 1). This Congo Craton also comprises the Mont Crystal, North Gabonese domain, and Chaillu massif in southern Gabon (Feybesse et al. 1998; Thiéblemont et al. 2018). The Oubanguide Complex or North Equatorial Fold Belt is the result of the Neoproterozoic collision between the Congo, West African, and Saharan shields (Feybesse et al. 1998; Caxito et al. 2020). The Ntem Complex, also known as the Ntem-Chaillu Block (Thiéblemont et al. 2018), is one of the ancient domains of the NW Congo Craton. The Edea region (Fig. 1) found

between latitudes 3°45' and 3°50' N and between longitudes 10° 05' and 10° 10' E belongs to the Nyong Complex.

The Ntem Complex consists of the Archean Tonalite-Trondhjemite-Granodiorite (TTG) dated at 2.9 Ga (Toteu et al. 1994), high-grade metamorphic hypersthene gneisses (charnockites, charno-enderbites, enderbites) and migmatites, as well as narrow and elongated greenstone-BIF. All intruded by extensive late K-rich granitoids (2.7–2.5 Ga; Tchameni et al. 2000; Shang et al. 2001, 2010) and contain large xenoliths of supracrustal rocks that are interpreted as remnants of greenstone belts and dated at 3.1 Ga (Tchameni et al. 2004). The deposition of the Ntem supracrustal formations is dated between 3.04 and 2.88 Ga (Tchameni et al. 2004; Thiéblemont et al. 2018). U–Pb zircon ages indicate the emplacement of charnockites and TTG between ca 3266 and ca. 2850 Ma (Toteu et al. 1994; Takam et al. 2009; Tchameni et al. 2010; Li et al. 2016; Akame et al. 2020a), while the associated mafic rocks crystallized at ca. 2.86 Ga (Li et al. 2016; Akame et al. 2020a). The late magmatic event in the Ntem Complex is represented by late high-K granitic intrusion dated at ca. 2666–2628 Ma (Tchameni et al. 2000). The Ntem Complex was affected by high thermal conditions of granulite and amphibolite metamorphic facies (737 ± 50 °C; Tchameni et al. 2010): a first metamorphic event at ca. 2900 Ma and a second metamorphic event of Paleoproterozoic age (~2050 Ma: Toteu et al. 1994). However, the recent works by Akame et al. (2020a) in Sangmelima area indicate 2843 ± 7 Ma (LA-ICP-MS U–Pb zircon) as the age of the migmatization of TTG-gneiss and 2744 ± 31 Ma (garnet-whole rock Sm–Nd) as the age of the second anatexis event coeval with D₂ deformation (Akame et al. 2020a). The Ntem Complex was affected by two Archean deformation phases (D₁, D₂) and late D₃ Paleoproterozoic event ca 2.1–2.0 Ga (Feybesse et al. 1998; Tchameni et al. 2000; Owona et al. 2011; 2020). D₁ is marked by a N080°E to N120°E and NNW-trend subvertical foliation formed during the high-grade metamorphic condition (Akame et al. 2020b). D₂ deformation is represent by F₂ isoclinal folds and C₂ ductile shear zones. The Archean structural trends were reworked by N045°E to N-S brittle shear zones during the Paleoproterozoic orogeny (Maurizot et al. 1986; Feybesse et al. 1998; Owona et al. 2011; Akame et al. 2020b).

The Nyong Complex comprises metasedimentary and metavolcanic rocks, syn-tectonic to late tectonic granitoids and syenites (Pouclet et al. 2007; Ndema Mbongué et al. 2014). The rocks are further divided into four main groups: (i) metavolcanic sedimentary rocks, probably remnants of greenstone belts, with orthopyroxene-bearing gneiss, garnet-rich amphibole-pyroxenite and related gneiss, banded iron formation, and mafic–ultramafic meta-volcanic rocks. The metavolcanic rocks were derived from the fractional crystallization of the same parental magma. Zircon U–Pb data revealed that the rhyodacite rocks initially formed

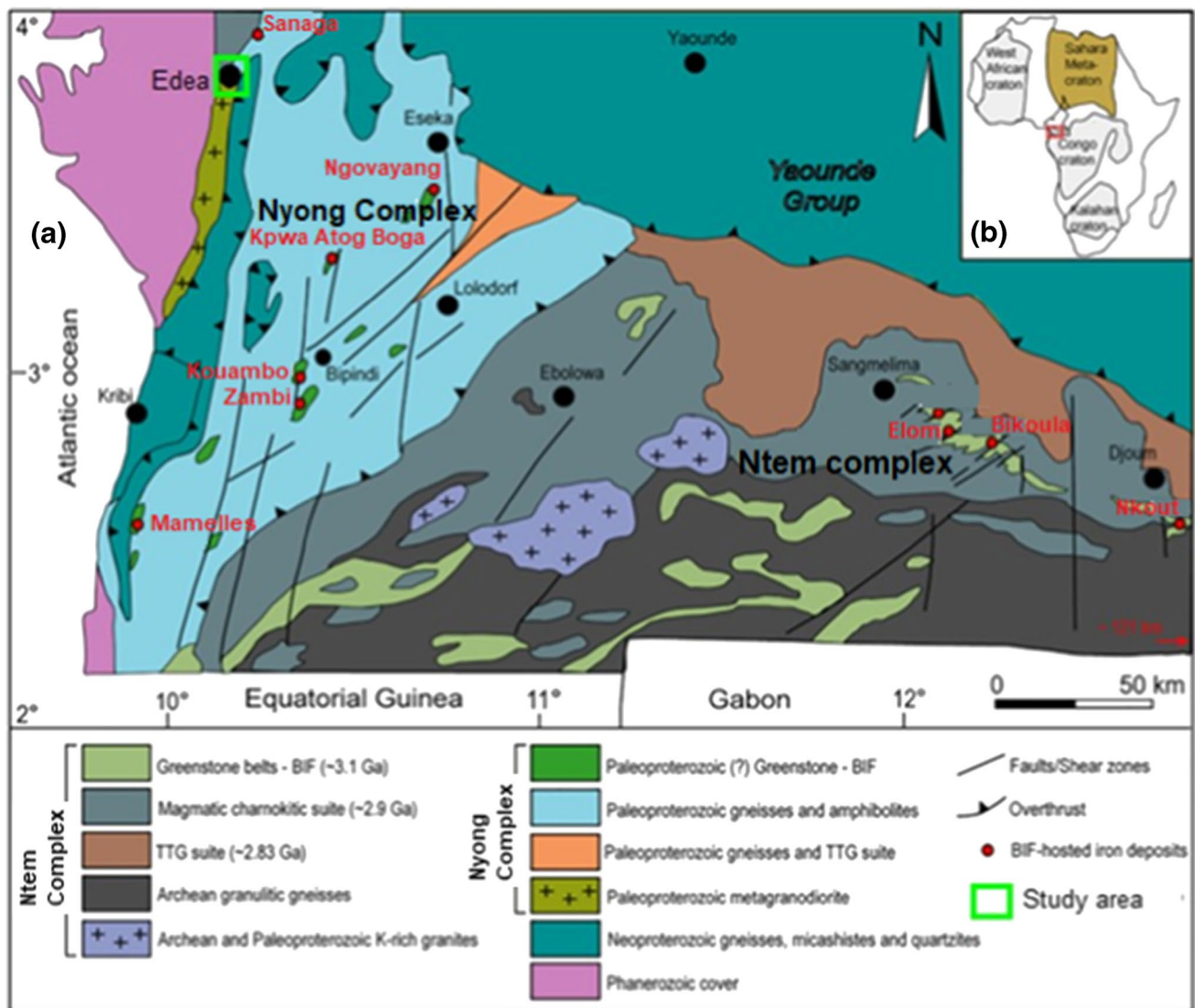


Fig. 1 a Geologic map of South-West Cameroon as modified from Maurizot et al. (1986) showing the lithologic units of Ntem Complex or Congo craton in Cameroon and the studied area (green box); b

sketch map of Africa showing African Cratons and the position of the Ntem Complex in the Congo craton (red box)

at 2671 ± 51 Ma and underwent later metamorphism at 2065 ± 55 Ma (Mvodo et al. 2022); (ii) migmatitic grey gneiss of tonalite–trondhjemite–granodiorite (TTG) composition; (iii) syn-tectonic to late-tectonic charnockite, granodioritic, augen gneiss, granite, and syenite; (iv) post tectonic meta-dolerite (Maurizot et al. 1986; Penaye et al. 2004; Owona et al. 2012; Chombong et al. 2017). Intrusions of metadiorites, granodiorites, and syenites cut rocks of the Nyong Complex, along with post-tectonic dolerites (Toteu et al. 1994; Lerouge et al. 2006; Nsifa Nkonguin et al. 2013). Three groups of ages are recorded into this Complex (Toteu et al. 1994; 2001; Lerouge et al. 2006): (1) Archaean ages (2500–2900 Ma), (2) Palaeoproterozoic (2050 Ma), and (3) Neoproterozoic (626 ± 26 Ma) ages.

Recent geochronological studies of detrital zircons from BIFs constrained the maximum depositional age of the Nyong Complex at 2422 ± 50 Ma (Soh Tamehe et al. 2021) or 2466 ± 62 Ma (Djoukouo Soh et al. 2021), while Owona et al. (2021a, 2021b) bracketed the deposition of the Nyong Complex between 2.4 and 2.2 Ga. Metasiliciclastic rocks and BIFs were deposited between ca. 2.1 and 2.0 Ga (Soh Tamehe et al. 2022) in a foreland basin developed along the northwestern continental margin of the East Gabonian Block. High-grade metamorphism is widespread within the Nyong Complex, coeval with tectonic emplacement of plutonic rocks (Toteu et al. 1994; Lerouge et al. 2006; Owona et al. 2020), whereas the aforementioned Archaean to Paleoproterozoic metasedimentary and metaigneous rocks have

also recorded Neoproterozoic imprints at ca. 600 Ma (Toteu et al. 1994; 2006; Chombong et al. 2017; Nzepang Tankwa et al. 2021; Owona et al. 2021a), interpreted as the Pan-African disturbance event.

The metasedimentary and metaplutonic rocks of the Nyong Complex have undergone a granulite facies metamorphism at 2100–2000 Ma and 2055 ± 5 Ma (SHRIMP U–Pb ages on zircons from metasedimentary and metaplutonic rocks; Lerouge et al. 2006), respectively, associated with the intrusion of charnockitic rocks (Toteu et al. 1994; Lerouge et al. 2006). The emplacement of these plutonic rocks within the Nyong Group is associated with Eburnean high-grade metamorphism which continued probably to 1985 ± 8 Ma (Lerouge et al. 2006). Toteu et al. (1994), and Lerouge et al. (2006) recorded non-Archean events by Eburnean zircon growth and titanite ages. Thus, the Nyong Complex recorded Paleoproterozoic and Pan-African reworking of the Archean Ntem Complex. Moreover, well-preserved to variably retrogressed eclogite facies metamorphic rocks dated at 2093 ± 45 Ma (SHRIMP U–Pb dating on zircon grains from eclogites) have been reported in the Nyong Complex (Loose and Schenk 2018; Bouyo Houketchang et al. 2019) suggesting that the subduction played during Paleoproterozoic as revealed by the SHRIMP zircon U–Pb eclogite facies metamorphism age of 2093 ± 45 Ma (Loose and Schenk 2018).

Structurally, the Nyong Complex shows a polyphase tectonic evolution (Ndema Mbongué et al. 2019a). It displays flat-lying foliations with N–S to NNE–SSW axial fold lineations and E–W to NW–SE stretching lineations that indicate an eastward-directed movement (Maurizot et al. 1986). The metasedimentary rocks display a composite, sub-vertical foliation ($S_{1/2}$), marked by alternating ferromagnesian and leucocratic layers (Feybesse et al. 1998) and the meta-granitoids contain the S_2 foliation. The entire Nyong Complex is dissected by NE-striking blastomylonitic shear zones (Owona et al. 2011). The relative large variety of igneous rocks and their structural and often high-grade metamorphic overprint require a clear assessment of their protolith and metamorphic ages to solidly tie their origin and reworking to the multi-stage orogenic evolution of western Central Africa (Loose and Schenk 2018; Bouyo Houketchang et al. 2019).

Geology of Edea area

The Edea area is located in the western part of the Nyong Complex in the northern margin of the Congo Craton. Few works have been done in the Edea area (Toteu et al. 1994; Lerouge et al. 2006; Ndema Mbongué et al. 2014; 2019a; 2019b; Moussango Ibohn et al. 2022). Lithologically, the study area is made up of a diversity of rock types that imply a diversity of the rock source. Some of these rocks include orthopyroxene garnet gneiss, charnockite, migmatite, and metagranodiorite showing features of mylonitization

(Kouankap Nono et al. 2018), metadiorite, garnet charnockitic gneiss, pyroxene gneiss, biotite gneiss, amphibolite, pyrobolite, pyrigarnite, charnockitic gneiss, micaschist, garnet-kyanite gneiss, and Pan-African syenite. Ndema Mbongué et al. (2014), Ndema Mbongué (2016), and Ndema Mbongué et al. (2019b) classified the rocks of the study area into three main units: (i) a unit of meta-igneous rocks, (ii) a metasedimentary rock unit, and (iii) the rocks resulting from the melt. The metaigneous rocks were derived from (i) intermediate to mafic tholeiitic rocks compatible with the extensive orogenic domain and (ii) calc-alkaline protolith which is in accordance with the typical domain of collisional orogeny (Ndema Mbongué et al. 2014). The metasedimentary rocks have the composition of shale, and a continental environment can be envisaged for these metasedimentary rocks. Iron formations have been reported in the Edea North Area: Bienkop (Ilouga et al. 2017), Kopongo (Mbang Bonda et al. 2017), and Pout Njouma (Ndema Mbongué and Aroke 2020); they include of BIF, magnetite gneiss, magnetite amphibole gneiss, massive magnetite, and magnetite quartzite (itabirite).

The Edea area is affected by a Paleoproterozoic granulitic metamorphism and a Pan-African metamorphism of the amphibolite facies (Ndema Mbongué 2016). This area experienced a polyphase deformation resulting to a succession of several phases of deformation (Ndema Mbongué et al. 2019a): (i) an early stage (pre- D_1) phase corresponds to the relicts of an early schistosity preserved as inclusion trails in garnet and pyroxene crystals, immediately followed by (ii) two main stages (D_1 and D_2). D_1 evolved in tangential movements; it is typically ductile and characterized by a regional-scale S_1 mylonitic foliation associated with F_1 folds and a subhorizontal stretching lineation L_1 . The deformation style of the D_2 phase is heterogeneous affecting the previous D_1 fabric by transposition, and evolved in a trans-current tectonic regime. The late- D_2 deformation phase is underlined by brittle structures. Syn-tectonic and pre-tectonic granitoids in this area recorded a heterogeneous polyphase tectonic deformation influenced by the Sanaga fault (Moussango Ibohn et al. 2022).

Analytical methods

Detailed observations and sampling were essentially carried out by mapping. In this study, 30 thin sections of meta-igneous and metasedimentary rocks were studied. The analyses of Th, U, Pb, Ca, Si, LREE, and Y for calibrations of the mineral chemistry were carried out at Chair of Mineralogy, University of Erlangen-Nürnberg, on a JEOL JXA 8200 at 20 kV, 100 nA, and a beam size of 5 μm (Schulz et al. 2007a). Based on counting statistics, the errors (1σ) are 1.0%, 0.20%, and 1.30% for Pb, Th, and U, respectively. The following lines have been chosen: $L\alpha_1$ lines for La, Y,

and Ce; $L\beta_1$ for Pr, Sm, Nd, and Gd; and $K\alpha_1$ for P, Si, and Ca. As standards for REE analyses (Jarosewich and Boatner 1991; Donovan et al. 2003), orthophosphates of the Smithsonian Institution were used. Calibration of PbO was carried out on a vanadinite standard, while U was calibrated on an appropriate glass standard with 5 wt% UO_2 . Interference of $YL\gamma$ on the $PbM\alpha$ line was corrected by linear extrapolation after measuring several Pb-free yttrium glass standards proposed by Montel et al. (1996). The interference of $ThM\gamma$ on $UM\beta$ is corrected using a Th-glass standard. The interference of a Gd-line on $UM\beta$ needs correction when Gd_2O_3 in monazite is > 5 wt%. These parameters matched the analytical problems discussed in Jercinovic and Williams (2005) in the best way (Schulz et al. 2007a). Other possible sources of error, as standardization, matrix effect correction, $YL\gamma$ -on- $PbM\alpha$ correction, and instrumental drift were not taken into account. Microprobe analyses of selected monazites gotten by electron microprobe analysis (EMPA) are given in Supplementary Table S2 to Table S4.

In the study area, monazites are present both in meta-igneous rocks (garnet-charnockitic gneisses, biotite-gneisses) samples and in metasedimentary unit (garnet-micaschists). Two samples (sample ED4B and sample ED3D) of garnet-charnockitic gneisses and one sample of metasediments (sample M4) of garnet-micaschists were selected for EMPA on monazite in terms of major and minor elements. These samples were chosen because they are more enriched in monazite crystals than other samples. Selected samples of monazite textural relationships and internal structures that reflect chemical variations are provided in Figs. 3 and 4. Monazite mineral chemistry (Supplementary Table S2 to Table S4) is described within the context provided by the imaging back-scattered electrons (BSE: 20 kV and 100 nA).

Results

Petrography

The lithology of Edea area consists of meta-igneous (pyroxene-gneisses, garnet-charnockitic gneisses and biotite-gneisses) and metasedimentary (garnet-micaschists) rocks. Mineral abbreviation recommendations by the IUGS Subcommittee on the Systematics of Metamorphic Rocks are according to Siivola and Schmid (2007).

Pyroxene-gneisses

Pyroxene-gneisses (Fig. 2a) are one of the dominant rock types and occur as dome and block. They are fine to medium-grained and consist of dark-gray colored rocks displaying alternating millimeter to decimeter ferromagnesian and quartzo-feldspathic layers. They display granoblastic

and corona microstructures (Fig. 2b) and composed of quartz (20–25%), plagioclase (15%) displaying transformation in sericite and surrounded by quartz grains recrystallization; almond-shaped orthopyroxene (20–30%) displaying corona microstructure; hornblende (4%); biotite (10–13%); and ovoid garnet (6–10%) crystals displaying symplectitic association of $Hbl + Bt + Qtz + Pl$. Accessory minerals are rutile (2%).

Garnet-charnockitic gneisses and biotite-gneisses

Garnet-charnockitic gneisses (Fig. 2c) are medium-grained made up of quartz (20–30%), plagioclase ($< 5\%$) displaying $Qtz + Bt + Grt \pm Opx$ association, almond-shaped orthopyroxene crystals (15–20%) displaying corona microstructure composed of $Qtz + Pl + Opx \pm Bt$, biotite (10–15%), and garnet porphyroblasts (20–25%) surrounded by $Qtz + Pl + Bt$ -rich rim and sometimes in atoll (Fig. 2d) consisting of a dissolved core with $Bt + Qtz + Pl$ -rich inclusions. Monazite (2%; Fig. 2e) and oxides (rutile, 2%) are accessories minerals.

Biotite-gneisses (Fig. 2f) outcrop as dome; they include fine grained minerals with alternate quartzo-feldspathic and ferromagnesian segregations, and granoblastic microstructures (Fig. 2g). These rocks consist of quartz (25–30%), plagioclase (20–15%) displaying transformation in sericite, biotite (35–40%), and epidote (7%). Accessory phases (5%) consist of monazite and oxides (rutile).

Garnet-micaschists

Garnet-micaschists (Fig. 2h) outcrop as flagstones. They are fine to medium-grained with alternate quartzo-feldspathic and ferromagnesian layers. Granoblastic microstructures (Fig. 3a) prevail in this rock type but flaser and mylonitic ones are frequently observed. Garnet-micaschists are composed of biotite (10–15%), muscovite (15%), garnet porphyroblasts (25–29%), quartz (15–17%), and plagioclase (20–22%) surrounded by $Bt + Qtz$ and displaying transformation in sericite; accessory minerals (2%) are monazite and opaque minerals.

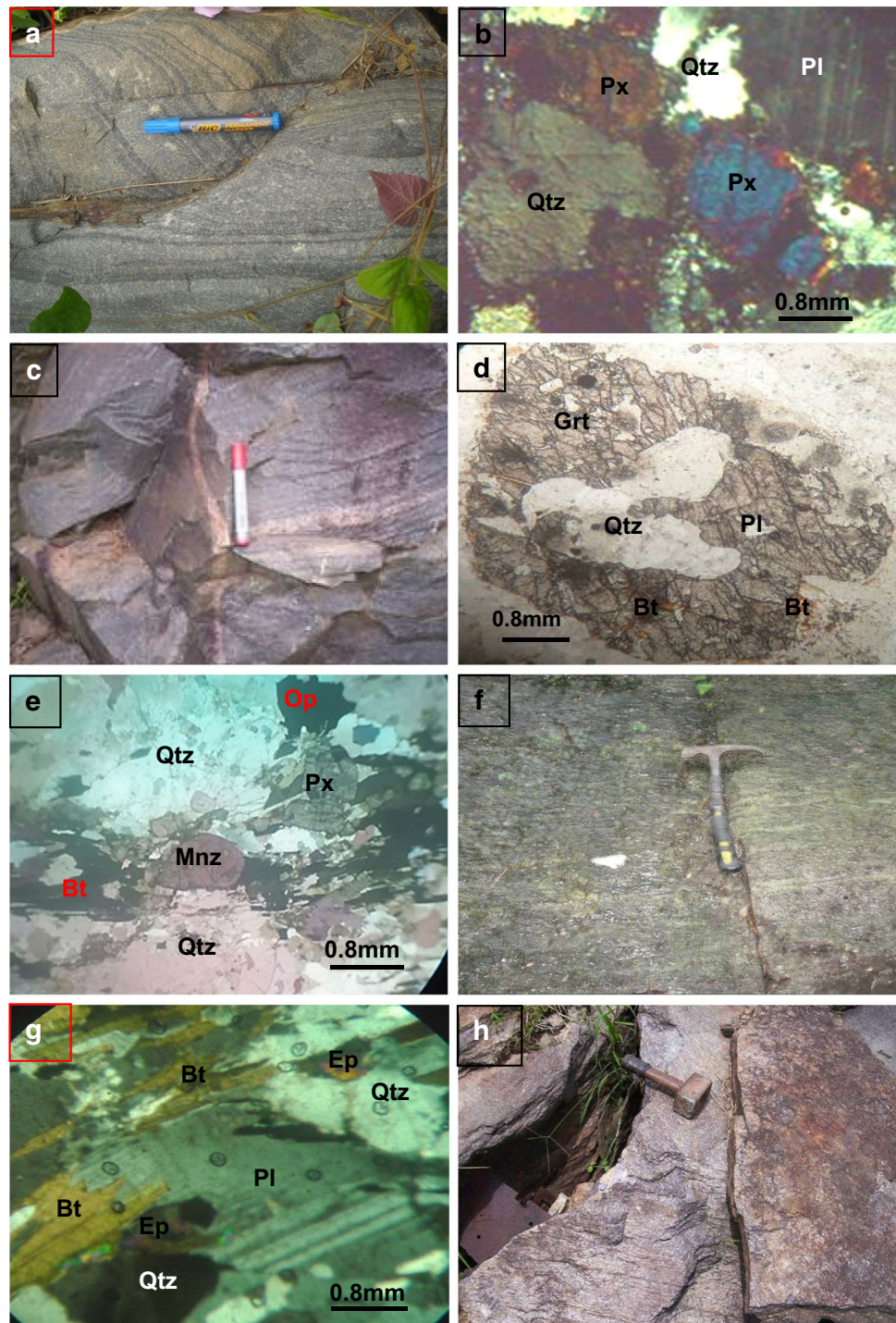
Textural characterization

Selected samples of monazite textural relationships and internal structures that reflect chemical variations are provided in Fig. 3 for meta-igneous rock samples and Fig. 4 for metasediments.

Monazites from meta-igneous rocks

In meta-igneous rock samples, the analyzed monazite crystals are of two main types: (i) elongated and oriented crystals

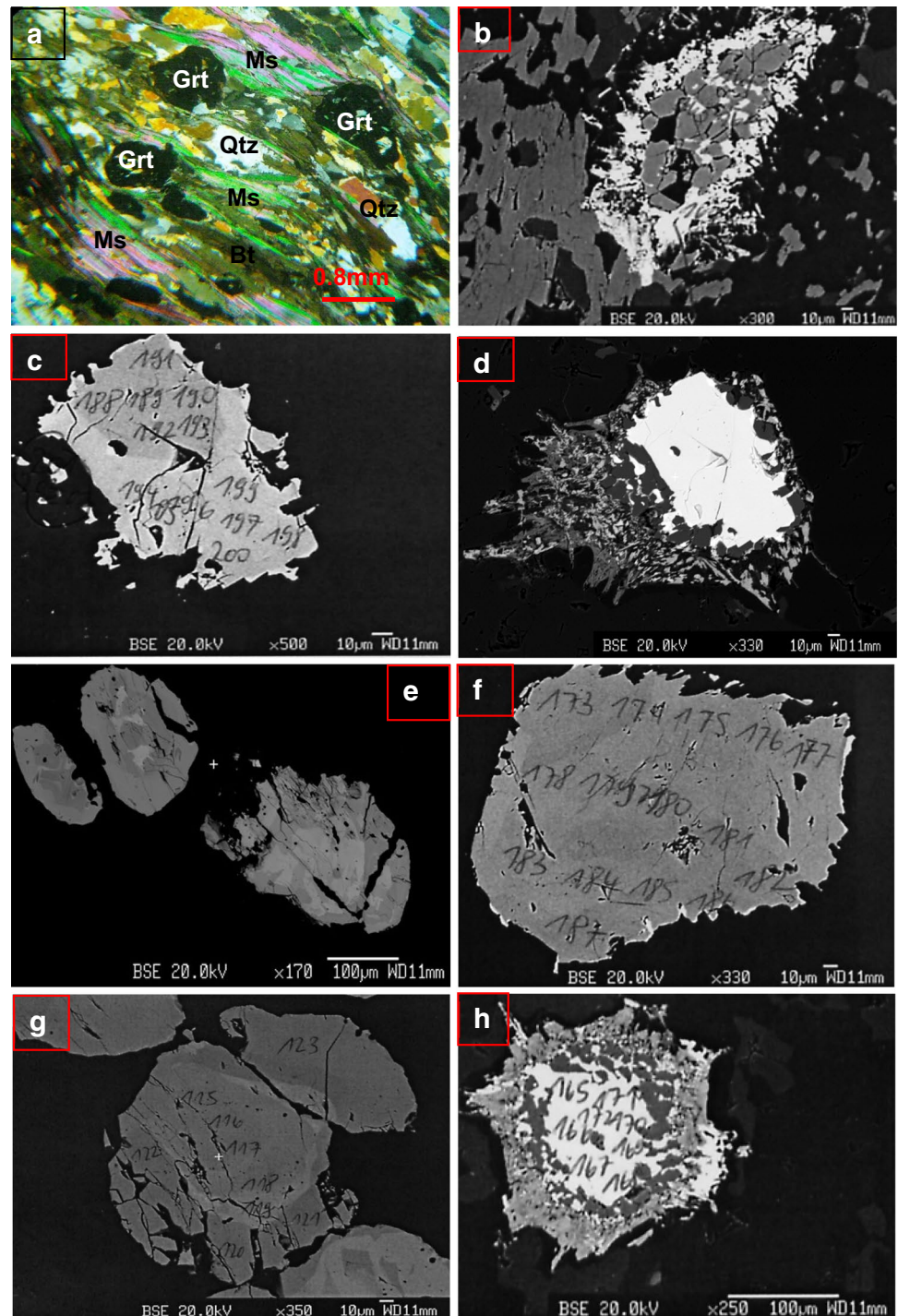
Fig. 2 Photographs and microphotographs of meta-igneous and metasedimentary rocks from the studied area. **a** Aspect of pyroxene-gneisses outcrop; **b** granoblastic and corona microstructures showing almond-shaped of Px surrounded by Qtz + Pl-rich rim pyroxene-gneisses; **c** garnet charnockitic gneisses field photograph; **d** atoll garnet consisting of Qtz + Pl dissolved core in the garnet charnockitic gneisses; **e** microphotograph of garnet charnockitic gneiss showing monazite crystal; **f** outcrop of biotite-gneisses; **g** granoblastic microstructures showing Bt + Pl + Qtz + Ep association in biotite-gneisses; **h** garnet-micaschists outcrop



(Figs. 3b, c and 3d, e), following the mylonitic foliation or schistosity (S_m or S_1) showing that these crystals are syn- S_m and characterizing the last phase of metamorphism (Ndema Mbongué et al. 2019a), and (ii) globular or ovoid crystals (Fig. 3f, g, h) constitute the earlier formed crystals which characterize the first phase of metamorphism. In BSE imaging (Fig. 3b–h), the monazite crystals are grey, bigger (200–325 μm in sample ED4B and 50–275 μm in sample

ED3D), and cracked. Some monazite grains display zoning and distinct dark grey and light grey domains (Fig. 3c, e, f, g) with a Th-enriched rim on textural older core. This observation implies that monazite crystallized from the melt liquid. In Fig. 3 b, d, and e, the analyzed monazite grains do not display any zonation. Some monazite crystals display a radiogenic halo (Fig. 3b, d, h) due to the radioactivity disintegration U-Th-Pb.

Fig. 3 Microphotograph of garnet-micaschist and back-scattered electron (BSE) images for analyzed monazite grains of meta-igneous rocks. **a** Granoblastic microstructure showing garnet porphyroblasts in the garnet-micaschists; **b, c, d, e** elongated and oriented crystal following the S_m -schistosity; **f, g, h** globular or ovoid shape crystals. Figures 3 c, e, f, and g display a zonation rim in Th

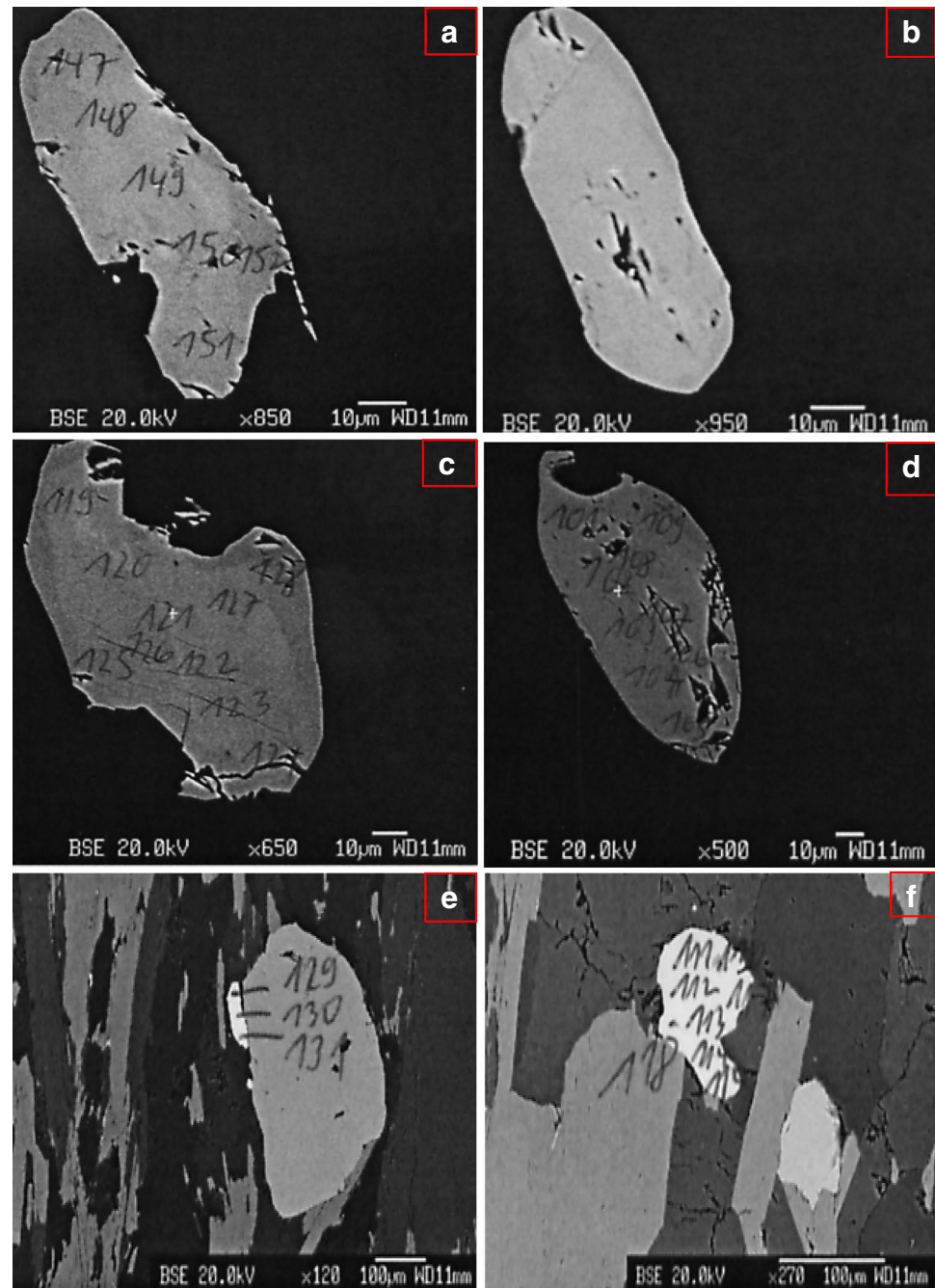


Monazites from metasedimentary rocks

The analyzed monazite grains (Fig. 4) from metasedimentary rocks (sample M4) display elongated (91 to 100 μm) and oriented crystals which mimic the S_2 schistosity (Fig. 4a to e; Ndema Mbongué et al. 2019a) characterizing the last phase of metamorphism, and ovoid grains (Fig. 4) which characterize the last phase of metamorphism. The orientation of

the monazite crystals following the S_2 schistosity, euhedral and sub-euhedral shape, and the homogeneity of the crystals suggests their metamorphic origin (Braun et al. 1998; Gonçalves et al. 2004; Gagné et al. 2009). Monazite crystals of metasediments are grey and cracked, and very well recrystallized. The BSE images of some monazite grains exhibit very clear zoning in Th along the monazite rims (Fig. 4a to d); these zonations are usually due to the variation in chemical

Fig. 4 Back-scattered electron (BSE) images of selected analyzed monazite crystals of metasedimentary rocks. **a, b, c, d, e** Elongated and oriented crystal following the S_2 schistosity; **f** globular or ovoid shape crystals. Note a zonation rim in Th in Figs. 4a–d



compositions. Monazite grains in Fig. 4 e and f do not display any zonation.

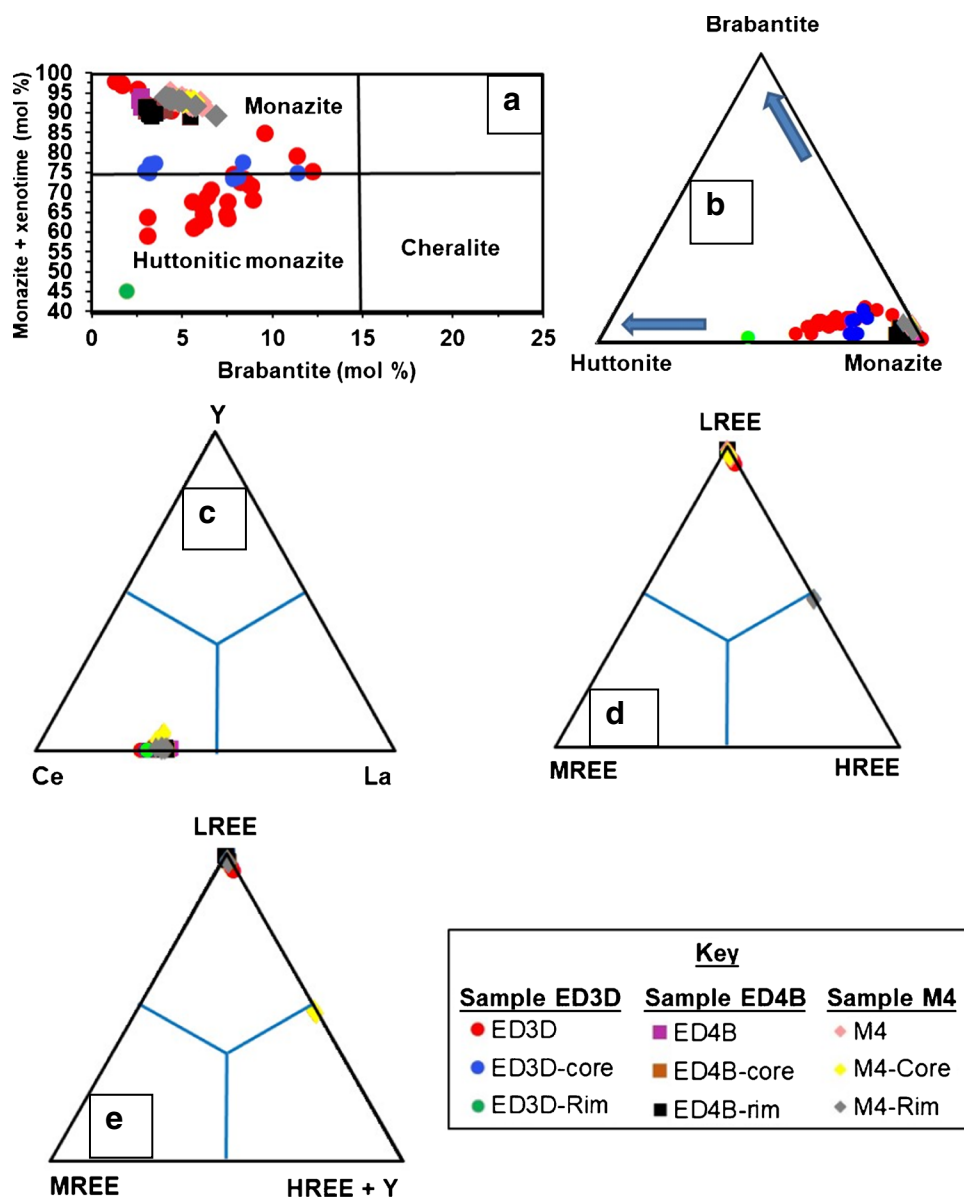
Mineral chemistry

Monazite composition

The composition of the analyzed monazite is presented in Supplementary Table S2 and Table S3 for the monazite of meta-igneous rocks (samples ED3D and ED4B respectively), and Supplementary Table S4 for the analyzed

monazite grains of metasediments (sample M4). A total of 124 spots have been analyzed: 78 spots in the monazite from meta-igneous rock samples (sample ED3D: 39 spots, sample ED4B: 39 spots) and 46 spots in the monazite of metasediments (sample M4). The chemical composition of monazite is not variable in the samples. The REE-bearing phase has been used to characterize the studied monazite from huttonitic monazite or cheralite (brabantite); therefore, in the plot of monazite + xenotime versus brabantite (Fig. 5a), majority of the analyzed spots, irrespective of core and rim for the analyzed grains of samples ED4B and

Fig. 5 Composition of monazites in meta-igneous rocks and metasediments from Edea area. The key should be applied for the whole text. **a** Composition of the analyzed monazite in the REE-bearing phase classification diagram monazite + xenotime (%) vs. cheralite (%); **b** plot of monazite composition in the huttonite-cheralite-monazite ternary system. Mole fraction is calculated after Perumalsamy et al. (2016). **c** Y-La-Ce, **d** LREE-HREE-MREE; **e** LREE-HREE + Y-MREE plots of the REE compositions for the analyzed monazite grains. LREE = $\sum(\text{La-Sm})$, MREE = Eu, HREE = Gd, HREE + Y = Gd + Y. The composition of monazite is normalized to 4 oxygens a.p.f.u. Note that the REE composition in monazite is note variable



M4, fall in the monazite field, with 85 to 98 mol% monazite content (Fig. 5a). The analyzed spots of sample ED3D fall in the field of huttonitic monazite (45 to 75 mol% monazite content) and monazite (75 to 98 mol% monazite content; Fig. 5a).

Distinct compositional differences, in terms of brabantite (or cheralite) content, are observed across the samples. Monazites in samples ED4B and M4 are chemically similar and characterized by low cheralite (Cher) or brabantite (Brb) content (<7 mol%) compared to the other spots that contain 8 to 16 mol% cheralite. Monazites from sample ED3D can be grouped into two dominant varieties (Fig. 5a) characterized by low cheralite (<5 mol%) and high monazite (75–98 mol%) and relative high cheralite (6–12 mol%) and low monazite (65–80 mol%). The xenotime solid solution

component in the analyzed monazites is low (sample ED3D (X_{Xen} : 0.3–5.2 mol%), sample ED4B (X_{Xen} : 0.3–2.0 mol%), and sample M4 (X_{Xen} : 1.7–6.2 mol%, av. = 2.53 mol%)) and includes Y (<0.012 a.p.f.u. for meta-igneous monazites and <0.04 a.p.f.u. for metasediment monazites), and Gd (<1.39 a.p.f.u. in meta-igneous monazites and <0.025 a.p.f.u. in metasediment monazites, Supplementary Table S2 to Table S4).

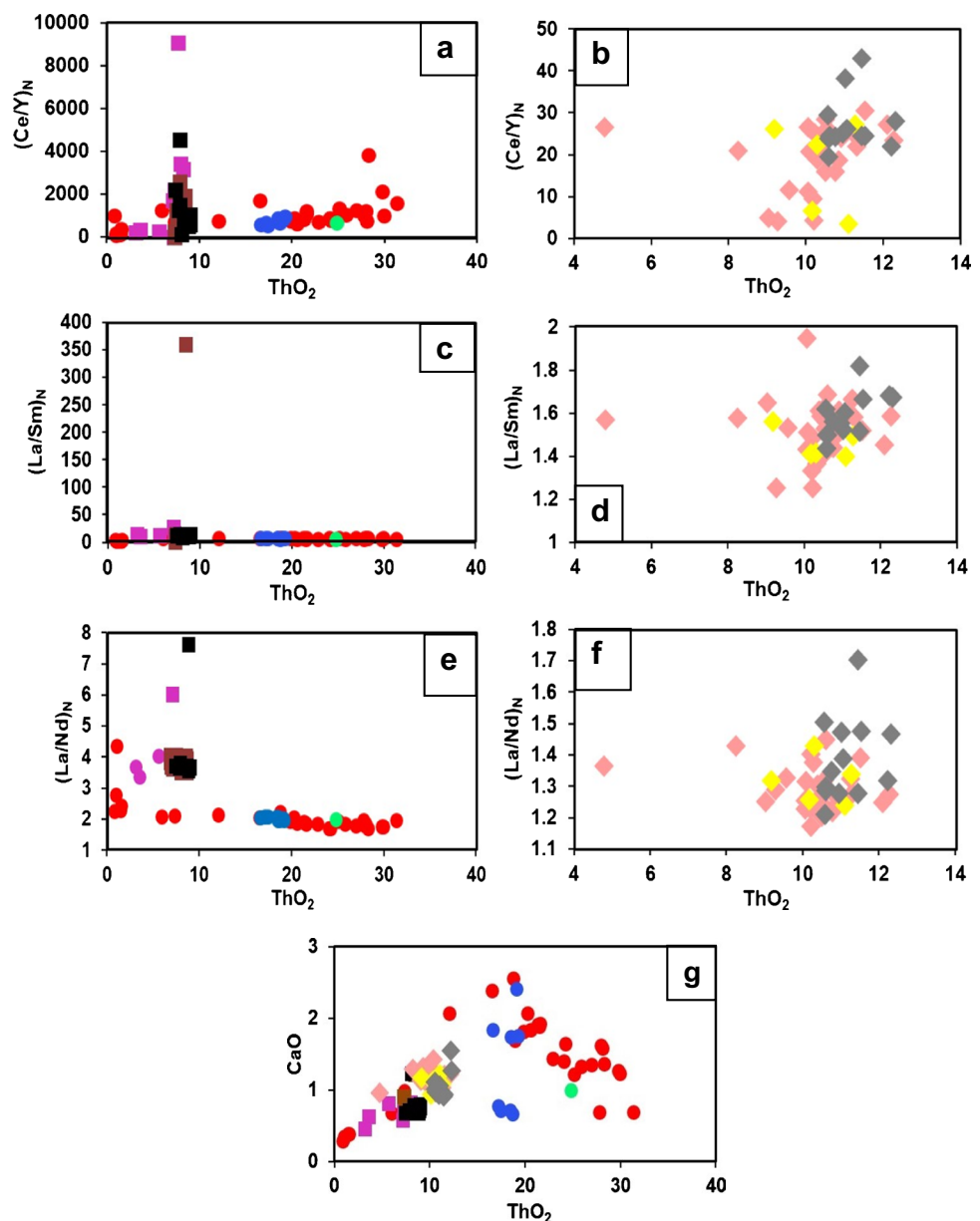
The mineral chemical data of monazite grains were plotted on a monazite–huttonite–brabantite ternary diagram (Fig. 5b). In this graph, the compositional of most of the analyzed monazite grains is dominantly linked with huttonitic substitution. All the analyzed monazite grains referred to monazite-(Ce) and exhibit a predominance of the LREE (Fig. 5c, d, e), with Ce (Fig. 5c) usually the dominant REE

(Ce = 0.26–0.46 a.p.f.u, Ce₂O₃ = 18.59 to 31.34%, av.: 23.19% in sample ED3D; for sample ED4B, Ce = 0.414–0.53 a.p.f.u, Ce₂O₃ = 23.35 to 32.6%, av.: 30.26%; and in sample M4, Ce = 0.38–0.45 a.p.f.u, Ce₂O₃ = 21.62 to 30.44%, av.: 29.23%). La₂O₃ (8–15.6%, av. = 10.43% in sample ED3D: 14.013–18.1%, av. = 17.20% for sample ED4B; 10.72–16.39%; av. = 15.70% in sample M4) contents are higher compared to poor SrO contents in sample ED3D (SrO = 0.11–0.15%), in sample ED4B (SrO = 0.113–0.152%) and in sample M4 (SrO = 0.13 to 0.18%).

Monazite is characterized by high ThO₂ contents that vary between 0.84 and 31.36% with an average of 18.79% in sample ED3D (Supplementary Table S2), 3.17 to 9.00% (av. = 7.70% in sample ED4B; Supplementary Table S3), 4.28 to 8.32% (av. = 5.48% for sample M4; Supplementary

Table S4), and broadly correlating with UO₂ which ranges from 0.3 to 0.95%, 0.097 to 1.45%, and 0.42 to 0.75%, respectively, for samples ED3D, ED4B, and M4. As a result, Th/U is high: 2.17–40.13 for sample ED3D, 5.7–36.23 in sample ED4B, and 8.44–12.6 in samples M4. This high Th/U is due to elevated Th contents (Supplementary Table S2, Table S3) in comparison with many published monazites (Dawood and Abd El-Naby 2007; Harley and Nandakumar 2014; Perumalsamy et al. 2016; Akame et al. 2021). Y₂O₃ is correspondingly low and inversely correlated with ThO₂ (Supplementary Table S2 to Table S4). The full range in Ce_N/Y_N is mostly in the range of 93.44–3845.95 for sample ED3D, 0.18–9069.27 for sample ED4B, and 3.55–43.07 for sample M4 (Fig. 6a, b). La_N/Sm_N is highly variable, from 2.38 to 8.01 in sample

Fig. 6 Chemical diagnostics of Edea monazite in relation to ThO₂ contents. **a** (Ce/Y)_N vs. ThO₂ plot meta-igneous monazite grains; **b** (Ce/Y)_N vs. ThO₂ plot for metasediments monazite grains; **c**) normalized (La/Sm)_N vs. ThO₂ diagram of meta-igneous monazites; **d** normalized (La/Sm)_N vs. ThO₂ diagram of metasediment monazites; **e** (La/Nd)_N vs. ThO₂ plot of meta-igneous monazites; **f** (La/Nd)_N vs. ThO₂ plot of metasediment monazites. Chondrite values used for normalization of meta-igneous monazite and metasediment monazite grains are from Anders and Grevesse (1989) and from Taylor and McLennan (1985), respectively. **g** CaO vs. ThO₂ plot for all the analyzed monazite



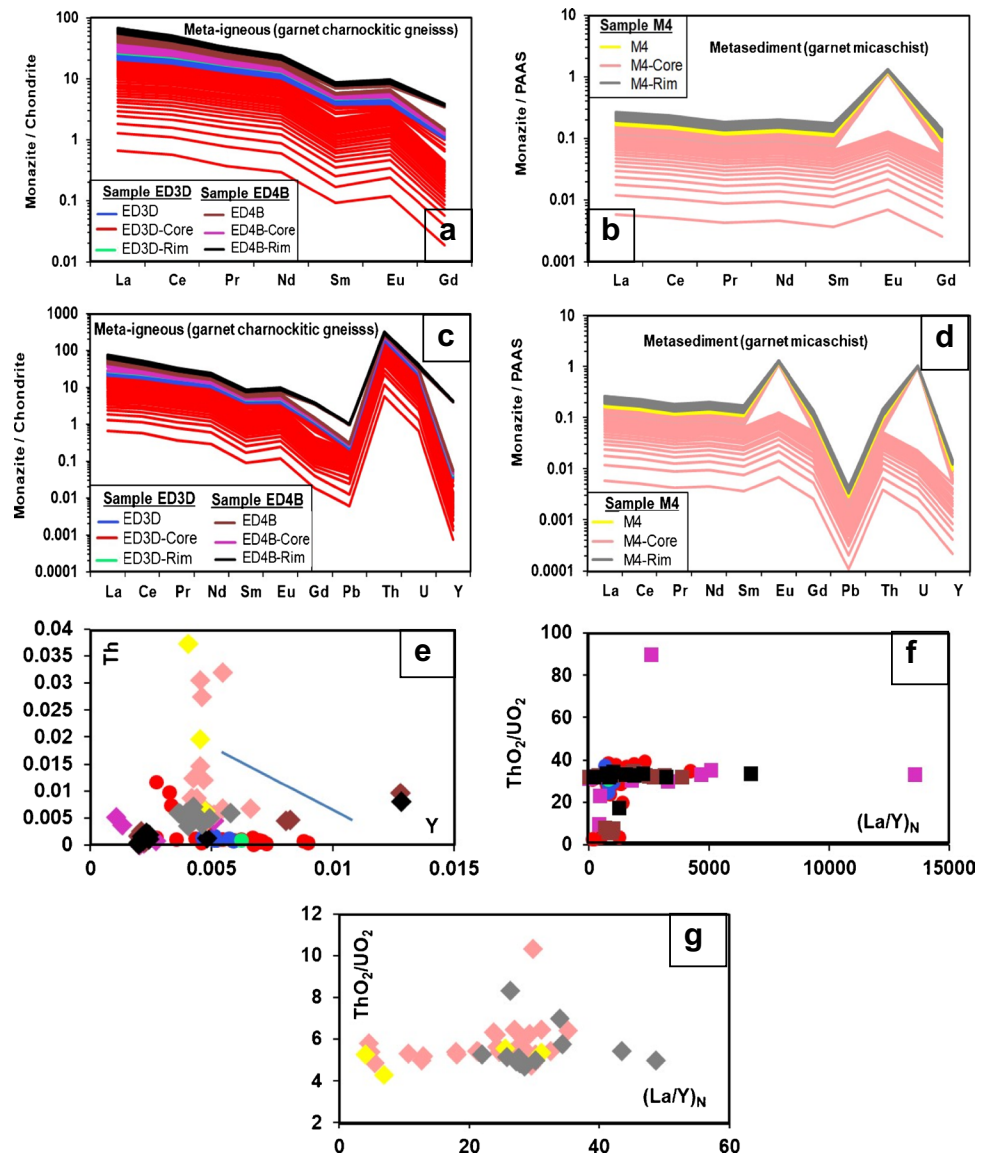
ED3D, 1.027 to 360.80 in sample ED4B, and less than 2 in sample M4 (Fig. 6c, 6d), and they yield normal La/Nd ratios variable and slightly greater than 4 (Supplementary Table S2 to Table S4; Fig. 6e, f).

The P_2O_5 contents are higher with a total range of 18.44–29.45% (av. = 24.44%) and 22.22–30.03% (av. = 27.98%) for meta-igneous samples (samples ED3D, ED4B, respectively) and 26.07–31.26% (av. = 31.26%) for the metasediments compared to UO_2 , PbO, and Al_2O_3 that show depleted concentrations. CaO (mean = 1.33%, 0.76%, 1.22%, respectively, in samples ED3D, ED4B, and M4) displays low values in all the analyzed samples (Fig. 6g) indicating that monazite is not stable with the calc-silicate phases (Finger et al. 1998). Silicon (Si) contents are almost uniform across the samples and vary from 0.008 to 0.64 a.p.f.u in sample ED3D, 0.03 to 0.073 a.p.f.u in sample ED4B and 0.011 to 0.035 a.p.f.u in metasediments.

REE, U, Th, and Y distribution in monazite

With respect to formula units, the following order among the REE can be established: $Ce > La > Nd > Pr > Sm > Eu > Gd$ for meta-igneous monazites and $Ce > La > Nd > Pr > Sm > Gd > Eu$ for metasedimentary rocks. In the chondrite and PAAS-normalized plots (Fig. 7a, b), the monazite grains from the study area show similar enriched patterns represented by LREE ($La_N/Sm_N = 1.03\text{--}360.80$) in meta-igneous monazites (Fig. 7a) and ($La_N/Sm_N = 1.25\text{--}1.95$) in metasedimentary monazites (Fig. 7b) indicating variable fractionation of the LREE, with only Gd from the HREE. These patterns (Fig. 7a, b) show a marked positive Eu anomaly for both meta-igneous ($Eu/Eu^* = 0.56\text{--}4.04$; mean = 2.77) and metasediment ($Eu/Eu^* = 1.56\text{--}2.54$) monazites, a positive Nd anomaly for meta-igneous monazites ($Nd/Nd^* = 0.42\text{--}8.26$; mean = 1.63), and null to slightly

Fig. 7 Chemical composition of Edea monazites. **a** Chondrite-normalized REE patterns for meta-igneous monazite grains; **b** PAAS-normalized REE patterns for metasediment monazites grains; **c** chondrite normalized spider diagram for meta-igneous monazite grains; **d** PAAS normalized spider diagram for metasediment monazites; **e** Th-Y binary plot for the analyzed monazite grains from Edea area; **f** plot of ThO_2/UO_2 vs. $(La/Y)_N$ of monazite from meta-igneous rocks; **g** Plot of ThO_2/UO_2 vs. $(La/Y)_N$ of monazite from metasediments



positive Nd anomaly for metasediment monazites ($Nd/Nd^* = 1.06\text{--}1.31$). These features are related to the associated minerals.

Chondrites (for samples ED3D, ED4B) and PAAS (for sample M4) normalized REEs, U, Th, Pb, and Y spider diagrams (Fig. 7c and d) reveal enrichment of LREEs over HREEs and distinct peak for Th (Fig. 7c) for the monazite from meta-igneous rock samples (samples ED3D, ED4B), and distinct peak for U (Fig. 7d) for the analyzed monazite grains of metasedimentary rock samples irrespective of core and rim domain. LREE fractionation decreases systematically with increasing ThO_2 and depleted in U. The Y and Th concentrations are depleted in a scatter-plot (Fig. 7e), indicating that monazite is depleted in Y relative to Th; monazite is also depleted in Y from the core relative to the rim and mostly enriched in Th as well. Distinctive samples exhibit very weak variation in Y contents that correlates inversely with Th (Fig. 7e); this is due to cheralite (brabantite) type of substitution in monazite: $2REE^{3+} = (Th,U)^{4+} + Ca^{2+}$ or $2REE = Th + Ca$ (Förster 1998; Nagy and Draganits 1999; Linthout 2007).

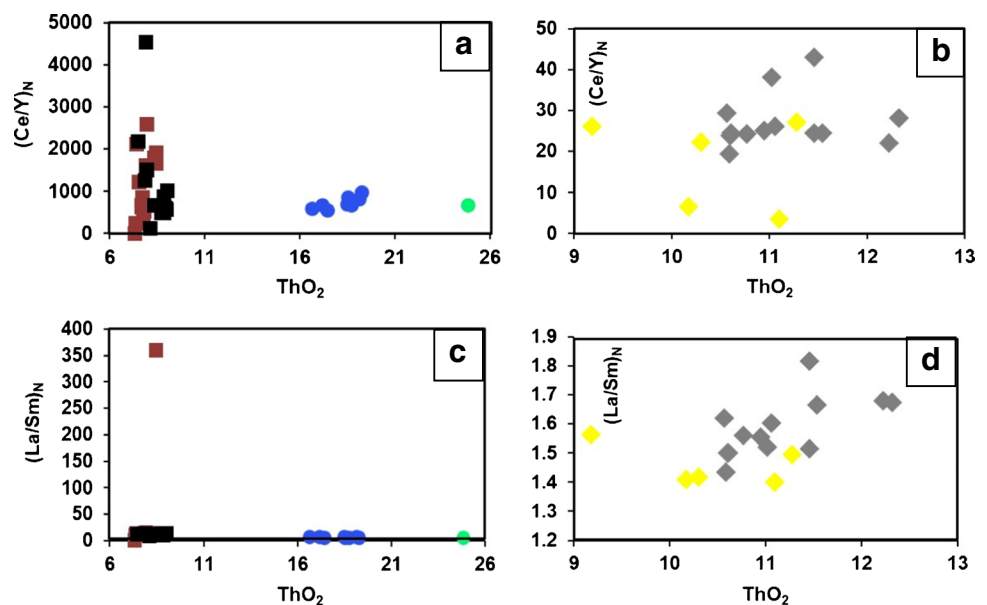
The normalized $(La/Y)_N$ ratio is plotted against ThO_2/UO_2 (Fig. 7f, g). On these diagrams, monazite from meta-igneous rock samples cluster around the chondrite values of La_N/Y_N ranging from 0 to 5000, with variable ThO_2/UO_2 ratios (0–40). The metasediment monazite samples define a wide variability with La_N/Y_N ratios varying from 0 to 50 and ThO_2/UO_2 ratios from 0 to 8. However, in all the three samples, Y concentrations and HREE contents are lower in the monazite grains. Also, the plots (Fig. 7f, g) show that monazite grains are more HREE-depleted relative to chondrite for samples ED4B, ED3D (Fig. 7c) and relative to PAAS for sample M4 (Fig. 7d), and monazites from both

rocks unit exhibit elevated $(La/Y)_N$ ratio (Supplementary Table S2, Table S2S2).

Chemical variation in the composition of monazite

In back scattered electron (BSE) images, the analyzed monazites are characterized by the variation in gray shades that reveal either concentric type of patchy type zoning pattern, with high Th, Y, and low Ce zones occurring as isolated patches within low Th, Y, and high Ce. In the zoning-type (Fig. 3b, c) observed in sample ED4B, dark gray shaded core domain is mantled by light gray shaded rim domain. The dark gray core domains have ThO_2 in the range of 16.62–19.22% in sample ED3D, 7.29 to 8.42% in sample ED4B, and 9.18–11.28% in sample M4. UO_2 clusters in the range of 0.52–0.66% in sample ED3D, 0.23 to 1.46% in sample ED4B, and 0.41–0.55% in sample M4. The range in Th/U ratio is 29.88–33.72 for sample ED3D, 5.92–34.60 in sample ED4B, and 10.40–11.53 in sample M4. Ce_N/Y_N is highly variable in the core and yields 551.70–979.72 in sample ED3D, 0.18 to 2549.01 in sample ED4B, and 3.55–27.16 in sample M4 (Fig. 8a, b). La_N/Sm_N displays constant values in the core (6.30–7.23 in sample ED3D and 1.40–1.56 in sample M4; except in sample ED4B that it varies from 1.03 to 360.80, with spot 183-C showing the highest value (360.80; Fig. 8c, d), with a mean of huttonite/brabantite ratio near 4.15, 1.78, and 0.38 in samples ED3D, ED4B, and M4, respectively. Dark gray core and light gray rim have a flat LREE pattern irrespective of ThO_2 (Fig. 8a, c), whereas ED4B-cores and ED4B-rim (Fig. 8a) with the lowest ThO_2 are enriched in Ce relative to Y. This may reflect their earlier crystallization from LREE-enriched melt.

Fig. 8 Core to rim monazite chemical diagnostics in relation to ThO_2 contents. **a, b** Ce_N/Y_N vs. ThO_2 plot for the textural compositional variation of monazite from meta-igneous rock (ED3D and ED4B) and monazite from metasediments (M4), respectively. ED4B-core and ED4B-rim conform to a trend to higher Ce_N/Y_N with increasing ThO_2 . **c, d** Plots of monazite $(La_N/Sm)_N$ vs. ThO_2 for the textural compositional variation of monazite from meta-igneous rock (ED3D and ED4B) and monazite from metasediments (M4), respectively



In patchy zoning, observed in samples ED4B (Fig. 3f), ED3D (Fig. 3g) and M4 (Fig. 4e, c), light gray patches of different shapes are hosted in dark gray matrix that comprises the dominant variant. Light gray BSE rim domains have high ThO_2 (24.80% for sample ED3D; 7.45–9.00% in sample ED4B and less than 1.82% in sample M4), Ce_N/Y_N greater than 680 in sample ED3D and strongly variable in sample ED4B (134.06–4549.90, and variable from 19.45 to 43.07 for sample M4 (Fig. 8a, b)). Y_2O_3 is less than 0.383% for all the core. UO_2 shows low contents in sample ED3D (0.80%) and in sample M4 (0.42–0.68%); it is very variable in sample ED4B (0.23–1451%), leading to elevated Th/U yielding 31.63, 5.70–35.74, and 10.80–12.60, respectively, for samples (ED3D, ED4B, and M4). These high-Th rims are relatively depleted in Y and HREE compared with the lower ThO_2 of the core domain. La_N/Sm_N is consistently low (6.38, 9.64–14.04, 1.43–1.82, respectively, in samples ED3D, ED4B, and M4 Fig. 8c, d), and the average huttonite/brabantite ratio is elevated in sample ED3D (27.38) and near 2 in sample ED4B and 0.48 for sample M4.

Discussion

Origin of monazite and metamorphic grade assessment

Monazites in the Edea area have been recorded in meta-igneous and metasedimentary rocks. These rocks contain garnet, amphibole, pyroxene, feldspar, biotite as main minerals, and monazite as accessory, suggesting that the sources of rare earth elements are major and accessory minerals. This result is in accordance with the studies by Kiesl et al. (1983), Bea (2015), and Ndema Mbongué et al. (2019b) indicating that the sources of rare earth elements and phosphorus in metamorphic rocks are major minerals or former accessory REE-minerals of the original rock, although migration of rare earth elements may also occur (Sawka et al. 1986).

Most of the studied monazites are generally elongated with the grain size varying from 50 to 325 μm for meta-igneous monazite grains and 91 to 100 μm for metasediment monazites. They display cracks which attest for the fluid-rock interactions (Braun et al. 1998). The internal structure that reflect chemical variations of the analyzed monazite is characterized by sharp and curve boundaries, suggesting a complex history with multiple episodes of dissolution and reprecipitation (Braun and Bröcker 2004; Ndema Mbongué 2016).

In the Si/Ce–Ca/Ce–Y/LREE ternary diagram (Wu et al. 2019), the majority of analyzed monazites plot in the field of metamorphic monazite (Fig. 9a), irrespective of core and rim domains, excepted some few grains from meta-igneous rocks (sample ED3D) and metasediments (sample M4) which fall within the field of igneous and metamorphic

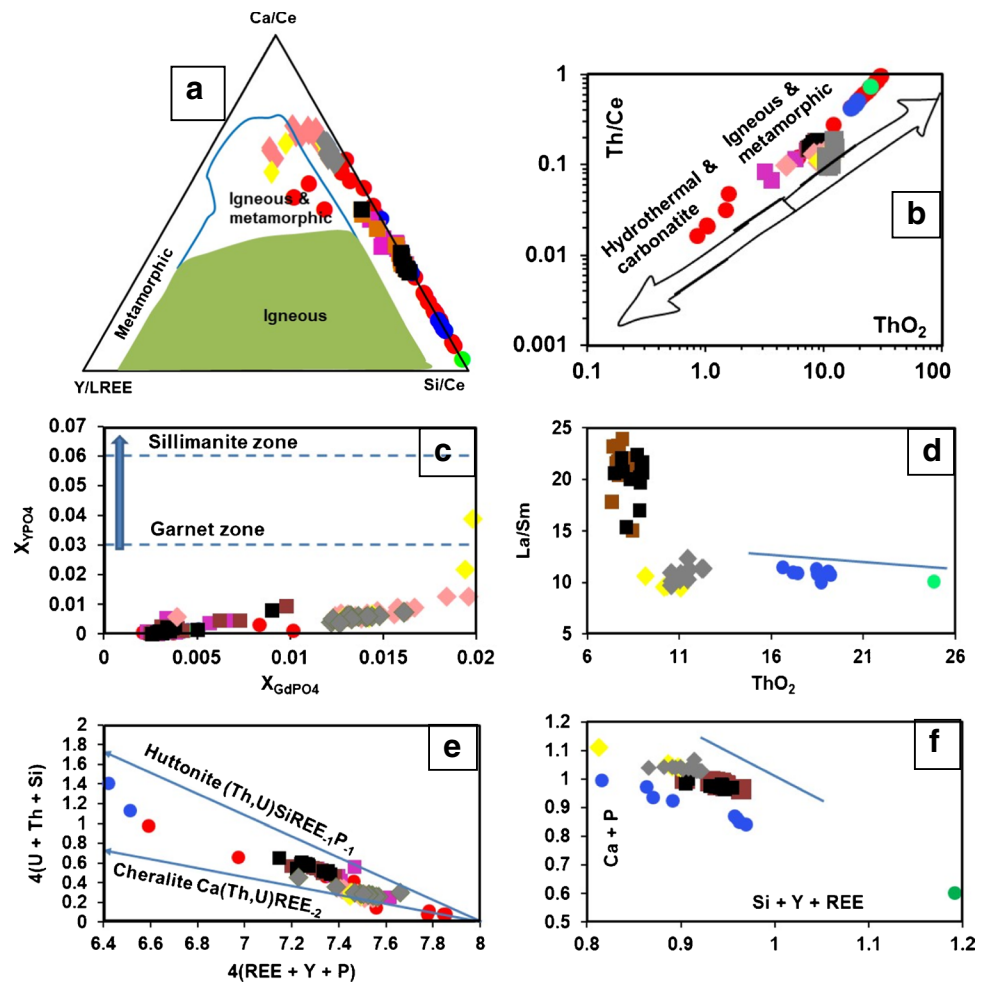
monazite. In addition, most of the analyzed monazites display low Th contents ($\text{Th} = 0.008\text{--}0.301$ a.p.f.u in sample ED3D; $\text{Th} = 0.031\text{--}0.085$ a.p.f.u for sample ED4B, $\text{Th} = 0.041\text{--}0.072$ a.p.f.u in sample M4) and low average Th/Ce ratios ($\text{Th}/\text{Ce} = 0.526$ in sample ED3D; $\text{Th}/\text{Ce} = 0.158$ for sample ED4B, $\text{Th}/\text{Ce} = 0.118$ in sample M4), and they plot into the field of igneous and metamorphic monazite in the Th/Ce versus ThO_2 plot (Fig. 9b), except some spots of samples ED3D that plot near to the field of hydrothermal or carbonatite monazite (Fig. 9b). Therefore, we suggest that the studied monazites are metamorphic monazites. Similar results were obtained for the monazite grains from Sangmelima area within the Congo Craton in Cameroon (Akame et al. 2021) and for the Diamantina monazite from Brazil (Didier et al. 2017; Gonçalves et al. 2018; Wu et al. 2019).

Due to their chemical constituents and their size (200–325 μm in sample ED4B, 50–275 μm in sample ED3D and 91 to 100 μm for sample M4), they characterize monazites from the high-grade metamorphic rocks (Schultz 2021) because monazites of high-grade metamorphic rocks are big (100 μm) compared to monazites in granites yielding between 20 and 50 μm (Franz et al. 1996; Montel et al. 1996; Malz 2001). With the increasing of metamorphic grade, the monazite grains tend to become bigger and more regular. La_2O_3 and Sm_2O_3 contents decrease, whilst Y_2O_3 concentrations increase with the increasing of metamorphic grade (Franz et al. 1996). Also, the HREE concentrations and the Y contents in monazite increase strongly with increasing metamorphic grade (Schultz 2021). The analyzed monazite grains have low X_{YPO_4} (≤ 0.02 mol; Supplementary Table S2 to Table S4; Fig. 9c) that fall below the limits of the garnet isograds as defined by Pyle et al. (2001) as X_{YPO_4} in monazite increases slightly with metamorphic grade. This result is different to one obtained by Akame et al. (2021).

The overall chemical composition of monazite from the Nyong Complex indicates higher Ce_2O_3 than other LREE, suggesting their classification as monazite-(Ce). They also display LREE-enrichment (e.g., La_2O_3 , Ce_2O_3 , Nd_2O_3) compared to HREE (e.g., Gd_2O_3), confirming that monazite crystal structure prefers to accommodate LREE than HREE since the concentration of HREE in monazite is < 0.02 per formula per 4 oxygens. Chondrite and PAAS-normalized REE patterns of the studied monazites show a marked positive Eu anomaly for both meta-igneous and metasediment monazites, a positive Nd anomaly for meta-igneous monazites ($\text{Nd}/\text{Nd}^* = 1.63$) and null to slightly positive Nd anomaly for metasediment monazites ($\text{Nd}/\text{Nd}^* = 1.06\text{--}1.31$). No Nd anomaly in REE data of pegmatites and granites are also reported by Förster (1998), Townsend et al. (2000), and Broška et al. (2005). The positive Eu in the analyzed monazites suggests plagioclase fractionation.

All monazite grains are characterized by high ThO_2 contents (av. = 8% for sample ED4B; 18% in sample ED3D, and

Fig. 9 Discrimination diagram of monazites. **a** Ternary diagram Si/Ce–Ca/Ce–Y/LREE showing the distribution of metamorphic monazites from Edea in the classification scheme of Wu et al. (2019); **b** monazite compositions plotted on Th vs. Th/Ce discrimination diagram. Igneous and metamorphic, hydrothermal and carbonatite monazite fields following classification scheme of Wu et al. (2019). **c** Monazite compositions in mole fractions of X_{GdPO_4} and X_{YPO_4} calculated according to Pyle et al. (2001). X_{YPO_4} in monazite increases with metamorphic grade. **d** La/Sm– ThO_2 variation diagram in the studied monazite grains. **e** Composition of monazite in $4(\text{U} + \text{Th} + \text{Si})$ vs. $4(\text{REE} + \text{Y} + \text{P})$ diagram normalized to 4 oxygens a.p.f.u, with ideal cheralite $\text{Ca}(\text{Th,U})\text{REE}_2$ and $(\text{Ca}, \text{Th,U})\text{Si}(\text{REE},\text{P})_1$ substitution vectors; **f** variation of $\text{Si} + \text{Y} + \text{REE}$ versus $\text{Ca} + \text{P}$. Note a negative correlation between $\text{Si} + \text{Y} + \text{REE}$ and $\text{Ca} + \text{P}$ for all the samples



5.5% in sample M4) and lower values of UO_2 (0.09–1.45%, 0.17–3%, and 0.42–0.7%, respectively) meaning that they refer to Th-rich monazites (Coates 1935; Dawood and Abd El-Naby 2007; Jaroslav 2010; Schultz 2021). Th-rich monazites are also reported from metamorphic rocks (Biljana et al. 2014) from low-T hydrothermal and metasomatic environments where they formed from the breakdown of primary REE-bearing phases (Poitrasson et al. 1996; 2000) and from placer deposits (Rupasinghe et al. 1983). Therefore, the studied monazite should be termed as Th-rich monazites-(Ce) because the average total content of ThO_2 in monazite is elevated in all the rock samples.

The high contents of ThO_2 can be correlated with the leucocratic minerals suggesting according to Gagné et al. (2009) that monazites have crystallized during the melt. La/Sm ratio is negatively weakly correlated with ThO_2 across core and rim in sample ED3D (Fig. 9d). La/Sm and ThO_2 content do not show any variation between core and rim in sample ED4B and sample M4. This can attest after Bhadra (2016) to armoring of the monazite grains of samples ED4B, ED3D, and M4 within the thick cordierite moat. Clustering of core composition of monazite from the textural domains

(Fig. 9d) suggests common heritage while lower La/Sm and highest ThO_2 can be related to late-phase melt crystallization processes (Bhadra 2016).

The average contents of P_2O_5 are not very different between the rock types; they consist of 28% and 24.36% in meta-igneous rocks (samples ED4B and ED3D respectively), and 30.25% for metasedimentary rock units (sample M4) with very low values of SiO_2 (0.78–1.80%, 0.21–9.08%, and 0.28–0.93%, respectively, in samples ED4B, ED3D, and M4). This indicates that a small quantity of Si occupies the tetrahedral site in the monazite structure. According to Biljana et al. (2014), the phosphorous necessary for monazite formation is supplied by a fluid phase. As shown by Krenn and Finger (2007), phosphorous can be mobile in low-T metamorphic fluids, which facilitates the in situ replacement of allanite by monazite.

The studied monazite has also integrated calcium because the compositions of the natural monazites vary in LREE, Th, Y, Ca, and Si (Franz et al. 1996). The decrease of Ca, HREE, Si, U, and Y and the increase of LREE indicate that chemical variation (core to rim variation) in the analyzed monazite grains is controlled by huttonite coupled-substitutions

($\text{LREE}^{3+} + \text{P}^{5+} = (\text{Th,U})^{4+} + \text{Si}^{4+}$; Van Emden et al. 1997; Zhu and O’Nions 1999; Harlov et al. 2007) and direct trivalent-ion substitution, rather than the cheralite substitution ($2\text{LREE}^{3+} = (\text{Th,U})^{4+} + \text{Ca}^{2+}$). Ca and Si are incorporated via these two reactions to balance the charge differences of the REE and actinides. Calcium occurs in the A site of the crystal structure of monazite, substituting for the slightly larger Ce ion, often concomitantly with the replacement of Ce by Th. Edea monazites are highly variable in U + Th + Si and REE chemistry, plotted in the $4(\text{U} + \text{Th} + \text{Si})$ vs. $4(\text{REE} + \text{Y} + \text{P})$ diagram (Fig. 9e); monazite compositions from all analyzed samples lie between the monazite–cheralite and monazite–huttonite trend lines irrespective of core and rim domains, indicating that the majority of Th + U can be accommodated by the two substitution mechanisms (Dawood and Abd El-Naby 2007). Therefore, we suggest that the Edea monazites are linked by dominantly huttonitic ($\text{LREE}^{3+} + \text{P}^{5+} = (\text{Th,U})^{4+} + \text{Si}^{4+}$) and cheralite ($2\text{LREE}^{3+} = (\text{Th,U})^{4+} + \text{Ca}^{2+}$) substitutions (Fig. 9e). These substitutions are very common in the studied monazite (Dawood and Abd El-Naby 2007; Harley and Nandakumar 2014; Perumalsamy et al. 2016; Bhadra 2016; Akame et al. 2021). The Edea monazite (75 to 95 mol% monazite; Fig. 5a), with dominantly huttonitic and cheralite substitutions (Fig. 5b) and variation in LREEs, MREEs (Eu), Th, U, and Pb (Fig. 7c, d) across the samples, suggests either a restricted source or identical thermal-metamorphic processes in the source regions of monazite in metamorphic rocks (Perumalsamy et al. 2016). The compositions of core and rim domains of monazites in the $\text{Ca} + \text{P}$ vs. $\text{Si} + \text{Y} + \text{REE}$ graph (Fig. 9f) which relates association of monazite and apatite through fluid substitution ($\text{Ca}^{2+} + \text{P}^{5+} + \text{fluid} = \text{Si}^{4+} + (\text{Y} + \text{REE})^{3+} + \text{fluid}$) indicate negative correlation for all samples. This suggests coeval growth of monazite and apatite (Bhadra 2016).

Monazite grains are characterized by low Y_2O_3 contents ($\leq 0.55\%$ for meta-igneous monazites, $\leq 1.86\%$ for metasediments samples) and low Y contents (≤ 0.012 a.p.f.u in meta-igneous monazites and ≤ 0.037 a.p.f.u in metasediment monazites) which is in accordance with low-Y monazite (Nagy and Draganits 1999; Schulz et al. 2007b; Holder et al. 2015).

Implications of the monazite chemistry on the metamorphic evolution of the Nyong Complex

Monazite microstructures of the Edea area are accompanied by the variable monazite mineral-chemical compositions; if this is combined with the in situ Th-U–Pb dating, it will provide a great potential to understand the monazite genesis and gives irreplaceable petrochronological constraints for the reconstruction of Nyong Complex. Textural relation of monazite grains and mineralogical observations

indicate that the studied rocks retain evidence of their poly-metamorphic history. The metamorphic evolution indicates that meta-igneous and metasediments of the study area are overprinted by two respective phases of metamorphism: in the meta-igneous rocks the first phase of metamorphism is underlined by globular or ovoid monazite grains and the second phase is characterized by elongated (50 to 325 μm) and oriented monazite crystals following the mylonitic foliation or schistosity (S_m or S_1). The first phase of metamorphism in metasedimentary rocks is marked by ovoid grains of monazite while the last phase is characterized by elongated (91 to 100 μm) and oriented monazites which mimic the S_2 schistosity. Both meta-igneous and metasediment monazites characterize monazites from the high grade metamorphic rocks confirming the widespread high-grade metamorphism in the Nyong Complex (Toteu et al. 1994; Lerouge et al. 2006; Owona et al. 2020).

The available literature indicates that the meta-igneous and metasedimentary rocks from the Nyong Group have suffered high-grade metamorphic at 2.05 Ga during Paleoproterozoic/Trans-Amazonian orogeny suggesting the existence of a major event with magmatism and charnockitization (Owona et al. 2021a; 2022; Soh Tamehe et al. 2022; Mvodo et al. 2022). The P–T conditions of the high-grade metamorphic of the Nyong Complex is estimated at ca 850 °C and 25 kb, while the retrograde conditions yielded ca 750 °C and 12 kb, suggesting a strong pressure drop of about 13 kb at nearly constant temperature during retrograde history and consequently to a rapid uplift (Bouyo Houketchang et al. 2019).

Conclusion

The main findings of this study with the implication of the monazite chemistry on the metamorphic evolution of the Nyong Group are listed below:

- The Edea monazite grains referred to Th-rich monazites (Ce) and exhibit a predominance of the LREE with Ce usually the dominant REE; they display zoning and distinct dark grey and light grey domains with a Th-enriched rim on textural older core. The compositions of core and rim domains of monazites reveal strong negative correlation suggesting coeval growth of monazite and apatite.
- Monazite compositions lie between the monazite–cheralite and monazite–huttonite trend lines suggesting they are linked by dominantly huttonitic and cheralite substitutions.
- The metamorphic evolution indicates that meta-igneous and metasediments of the Nyong Group are overprinted by two respective high grade phases of metamorphism: in the meta-igneous rocks, the first phase of metamorphism

is underlined by globular or ovoid monazite grains, and the second phase is characterized by elongated and oriented monazite crystals following the mylonitic foliation or schistosity (S_m or S_1). The first phase of metamorphism in metasediment is also marked by ovoid grains of monazite, while the last phase is characterized by elongated and oriented monazites which mimic the S_2 schistosity.

Supplementary Information The online version contains supplementary material available at <https://doi.org/10.1007/s12517-022-10924-7>.

Acknowledgements The authors are grateful to Chair of Mineralogy, University of Erlangen-Nürnberg (Germany) and especially Professor Bernhard Schulz for EMPA on monazite.

Declarations

Conflict of interest The authors declare no competing interests.

References

- Akame JM, Oliveira EP, Poujol M, Hublet G, Debaille V (2020a) LA-ICP-MS zircon U Pb dating, Lu Hf, Sm Nd geochronology and tectonic setting of the Mesoproterozoic mafic and felsic magmatic rocks in the Sangmelima granite-greenstone terrane, Ntem Complex (South Cameroon). *Lithos* 372–373:105702. <https://doi.org/10.1016/j.lithos.2020.105702>
- Akame JM, Owona S, Hublet G, Debaille V (2020b) Archean tectonics in the Sangmelima granite-greenstone terranes, Ntem Complex (NW Congo craton), southern Cameroon. *J Afr Earth Sci* 168:103872. <https://doi.org/10.1016/j.jafrearsci.2020.103872>
- Akame JM, Schulz B, Owona S, Debaille V (2021) Monazite EPMA-CHIME dating of Sangmelima granulite and granitoid rocks in the Ntem Complex, Cameroon: implications for Archean tectono-thermal evolution of NW Congo craton. *J Afr Earth Sci* 181:1–20
- Anders E, Grevesse N (1989) Abundance of elements: meteoritic and solar. *Geochim Cosmochim Acta* 53:197–214
- Bea F (2015) Geochemistry of the lanthanide elements. XXXV Reunión de la Sociedad Española de Mineralogía, Department of Mineralogy and Petrology, University of Granada pp 1–12
- Bhadra S (2016) Timing and duration of ultra-high temperature metamorphism in apphirine-bearing metapelite ghranulite from Kodaikanal, Madurai block, South India: constraints from mineral chemistry and U-Th-total Pb epmaage of monazite. *J Appl Geochem* 18(1):22–34
- Biljana SM, Krenn E, Finger F (2014) Microcrystals of Th-rich monazite (La) with a negative Ce anomaly in metadiorite and their role for documenting Cretaceous metamorphism in the Slavonian Mountains (Croatia). *Miner Petrol* 108:231–243
- Bouyou Houketchang M, Penaye J, Mouri H, Toteu SF (2019) Eclogite facies metabasites from the Paleoproterozoic Nyong Group, SW Cameroon: mineralogical evidence and implications for a highpressure metamorphism related to a subduction zone at the NW margin of the Archean Congo craton. *J Afr Earth Sc* 149:215–234
- Brandt S, Schenk V, Raith MM, Appel P, Gerdes A, Srikanthappa C (2011) Late Neoproterozoic P-T evolution of HP-UHT granulites from the Palni Hills (South India): new constraints from phase diagram modelling, LA-ICP-MS zircon dating and in-situ EMP monazite dating. *J Petrol* 52:1813–1856. <https://doi.org/10.1093/petrology/egr032>
- Braun I, Montel JM, Nicollet C (1998) Electron microprobe dating of monazites from high-grade gneisses and pegmatites of the Kerala Khondalite Belt, southern India. *Chem Geol* 146:65–85
- Braun I, Bröcker M (2004) Monazite dating of granitic gneiss and leucogranites from the Kerala Khondalite Belt, Southern India: implications for Late Prototrozoic crustal evolution in East Gondwana. *Int J Earth Sc (Geol Rundsch)* 93:13–22
- Breithaupt A (1829) Über den Monazit, eine neue Specie des Mineral Reichs. *J Chem Phys* 55:301–303
- Broska I, Williams CT, Janák M, Nagy G (2005) Alteration and breakdown of xenotime-(Y) and monazite-(Ce) in granitic rocks of the Western Carpathians, Slovakia. *Lithos* 82:71–83
- Caxito FA, Santos LCML, Ganade CE, Bendaoud A, Fettous EH, Bouyou Houketchang M (2020) Toward an integrated model of geological evolution for NE Brazil–NW Africa: the Borborema Province and its connections to the Trans-Saharan (Benino-Nigerian and Tuareg shields) and Central African orogens. Special session, “A tribute to Edilton Santos, a leader in Precambrian Geology in Northeastern Brazil”, edited by AN Sial and VP Ferreira. *Brazilian J Geol* 50(2):1–38. <https://doi.org/10.1590/2317-4889202020190122>
- Chombong NN, Suh CE, Lehmann B, Vishiti A, Ilouga DC, Shemang EM, Tantoh BS, Kedia AC (2017) Host rock geochemistry, texture and chemical composition of magnetite in iron ore in the Neoproterozoic Nyong unit in southern Cameroon. *Appl Earth Sci* 126:129–145
- Coates JS (1935) Geology of ceylon. *Ceylon J Sci (b)* 19(2):101–187
- Dahl SP, Terry MP, Jercinovic MJ, Williams MJ, Hamilton MA, Foland KA, Clement SM, Friberg LM (2005) Electron probe (ultrachron) microchronometry of metamorphic monazite: unraveling the timing of polyphase thermotectonism in the easternmost Wyoming Craton (Black hills, South Dakota). *Am Mineral* 90:1712–1728
- Dawood YH, Abd El-Naby HH (2007) Mineral chemistry of monazite from the black sand deposits, northern Sinai, Egypt: a provenance perspective. *Mineral Mag* 71(4):389–406
- Didier A, Pultitz B, Baumgartner LP, Bouvier AS, Vennemann TW (2017) Evaluation of potential monazite reference materials for oxygen isotope analyses by SIMS and laser assisted fluorination. *Chem Geol* 450:199–209. <https://doi.org/10.1016/j.chemgeo.2016.12.031>
- Djoukouo Soh AP, Ganno S, Zhang LC, Soh Tamehe L, Wang CL, Peng ZH, Tong XX, Nzenti JP (2021) Geochemical and geochronological constraints on the origin of the Bibole banded iron formations, northwestern Congo Craton Cameroon: implications for their depositional age and tectonic environment. *Geol Mag* 158:2245–2263. <https://doi.org/10.1017/S0016756821000765>
- Donovan JJ, Hanchar JM, Picolli PM, Schrier MD, Boatner LA, Jarosewich E (2003) A Re Examination of the rare-earth-element orthophosphate standards in use for electron microprobe analysis. *Can Mineral* 41(1):221–232. <https://doi.org/10.2113/gscanmin.41.1.221>
- Feybesse JL, Johan V, Triboulet C, Guerrot C, Mayaga-Mikolo F, Bouchot V, Eko NJ (1998) The West Central African belt: a model of 2.5–2.0 Ga accretion and two-phase orogenic evolution. *Prec Res* 87:161–216
- Finger F, Broska I, Roberts MP, Schermaier A (1998) Replacement of primary monazite by apatite-allanite-epidote coronas in an amphibolite facies granite gneiss from the eastern Apls. *Am Mineral* 83:248–258
- Förster HJ (1998) The chemical composition of REE–Y–Th–U-rich accessory minerals in peraluminous granites of the Erzgebirge-Fichtelgebirge region, Germany. I. The monazite-(Ce) – brabantite solid solution series. *Am Mineral* 83:259–272

- Foster GL, Parrish RR (2003) Metamorphic monazite and the generation of P–T–t paths, in: Vance D, Muller W, Villa IM (Ed) *Geochronology: linking the Isotopic Record with Petrology and Textures*. Geol Soc London Spec Publ. 220:25–47
- Franz G, Andrehs G, Rhede D (1996) Crystal chemistry of monazite and xenotime from Saxothuringian-Moldanubian metapelites, NE Bavaria, Germany. *Eur J Mineral* 8:1097–1118
- Gagné S, Jamieson RA, Mackay R (2009) Texture, composition, and age variations in monazite from the lower amphibolite to the granulite facies, longstaff bluff formation, Baffin Island, Canada. *The Can Mineral* 47:847–869
- Gardes E (2006) Diffusion du plomb dans la monazite. Thèse de doctorat, Université de Toulouse III
- Gonçalves GO, Lana C, Scholz R, Buick IS, Gerdes A, Kamo SL, Corfu F, Rubatto D, Wiedenbeck M, Nalini HA, Oliveira LCA (2018) The Diamantina monazite: a new low-Th reference material for microanalysis. *Geostand Geoanal Res* 42:25–47. <https://doi.org/10.1111/ggr.12192>
- Goncalves P, Nicollet C, Montel JM (2004) Petrology and insitu U–Th–Pb monazite geochronology of ultrahigh-temperature metamorphism from the Andriamena Mafic Unit, North–Central Madagascar. Significance of a petrographical P–T Path in a polymetamorphic context. *J Petrol* 1–35
- Harley SL, Nandakumar V (2014) Accessory mineral behaviour in granulite migmatites: a case study from the Kerala Khondalite Belt. *India J Petrol* 55(10):1965–2002
- Harlow DE, Wirth R, Hetherington CJ (2007) The relative stability of monazite and huttonite at 300–900°C and 200–1000 MPa: metasomatism and the propagation of metastable mineral phases. *Am Mineral* 92:1652–1664
- Harrison TM, Catlos EJ, Montel JM (2002) U–Th–Pb dating of phosphate minerals. *Rev Mineral Geochem* 48:524–558. <https://doi.org/10.2138/rmg.2002.48.14>
- Heinrich W, Andrehs G, Franz G (1997) Monazite-xenotime miscibility gap thermometry. I. An Empirical Calibration *J Metamorph Geol* 15:3–16
- Hobart MK (2018) Monazite: a rare phosphate mineral mined from placer deposits for its rare earth and thorium content. Retrieval from <https://geology.com/minerals/monazite.htm>. Accessed 16 Oct 2014
- Holder RM, Hacker BR, Kylander-Clark ARC, Cottle JM (2015) Monazite trace-element and isotopic signatures of (ultra)high-pressure metamorphism: examples from the Western Gneiss Region, Norway. *Chem Geol* 409:99–111
- Hughes JM., Foord EE, Hubbard MA, Ni Yunxiang (1995) The crystal structure of cheralite-(Ce), (LREE, Ca, Th, U)(P, Si)PO₄, a monazite-group mineral. *Neues Jahrb. Mineral Monatsh* 344–350
- Ilouga DCI, Ndong Bidzang F, Ziem A, Bidias LA, Olinga JB, Tata E, Minyem D (2017) Geochemical characterization of a stratigraphic log bearing iron ore in the Sanaga Prospect, Upper Nyong Unit of Ntem Complex, Cameroon. *J Geosci Geom* 5(5):218–228. <https://doi.org/10.12691/jgg-5-5-1>
- Jarosewich E, Boatner LA (1991) Rare-earth element reference samples for electron microprobe analysis. *Geostd News Lett* 15(2):397–399. <https://doi.org/10.1111/j.1751-908X.1991.tb00115.x>
- Jaroslav P (2010) Metamorphic-hydrothermal REE minerals in the Bacúch magnetite deposit, western Carpathians, Slovakia: (Sr, S)-rich monazite-(Ce) and Nd-dominant hingganite. *Can Mineral* 48:81–94. <https://doi.org/10.3749/canmin.48.1.81>
- Jercinovic MJ, Williams ML (2005) Analytical perils (and progress) in electron microprobe trace element analysis applied to geochronology: background acquisition, interferences, and beam irradiation effects. *Am Miner* 90(5):526–546. <https://doi.org/10.2138/am.2005.1422>
- Kiesel W, Wieseneder H, Kluger F (1983) Untersuchungen des Vorkommens der Seltenen Erden und von Thorium in Gesteinen des unteraustroalpinen Kristallins des Semmering- Wechselfensterns. - Sitzungsber Österr Akad Wiss Mathem-Naturwiss Kl, Abt I, 192/1–4:1–20
- Kouankap Nono GD, Njiosseu Tanko EL, Takodjou Wambo JD, Kamguia Woguia B, Afahnwie Ngambu A, Fomena Tchinda H, Folah Mewa CL (2018) Petro-structural characterization of Bonguen Area, Nyong Series, Cameroon: insight into the Northern Extension of Kribi–Campo Shear Zone. *Earth Sci* 7(5):236–241. <https://doi.org/10.11648/j.earth.20180705.15>
- Krenn E, Finger F (2007) Formation of monazite and rhabdophane at the expense of allanite during Alpine low temperature retrogression of metapelitic basement rocks from Crete, Greece: microprobe data and geochronological implications. *Lithos* 95:130–147
- Lerouge C, Cocherie A, Toteu SF, Penaye J, Milesi JP, Tchameni R, Nsifa NE, Fanning CM, Deloule E (2006) SHRIMP U/Pb zircon age evidence for paleoproterozoic sedimentation and 2.05Ga syntectonic plutonism in the Nyong Group, South-western Cameroon: consequences for the eburnean-transamazonian belt of NE Brasil and central Africa. *J Afric Earth Sci* 44:413–427
- Li XH, Chen Y, Li J, Yang C, Ling XX, Tchouankoue JP (2016) New isotopic constraints on age and origin of Mesoarchean charnockite, trondhjemite and amphibolite in the Ntem Complex of NW Congo Craton, southern Cameroon. *Prec Res* 276:14–23. <https://doi.org/10.1016/j.precamres.2016.01.027>
- Linthout K (2007) Tripartite division of the system 2REEPO₄–CaTh(PO₄)₂–2ThSiO₄, discreditation of brabantite, and recognition of cheralite as the name for members dominated by CaTh(PO₄)₂. *Can Mineral* 45:503–508
- Loose D, Schenk V (2018) 2.09 Ga old eclogites in the Eburnian-Transamazonian orogen of southern Cameroon: significance for Palaeoproterozoic plate tectonics. *Prec Res* 304:1–11
- Malz N (2001) Electron-microprobe dating of monazite. Institute of Mineralogy, TU Bergakademie Freiberg 1–11
- Maurizot P, Abessolo A, Feybesse A, Johan JL, Lecomte P (1986) Etude et prospection minière du Sud-Cameroun. Synthèse des travaux de 1978 à 1985. Rapport BRGM, 85. Cameroon 066:224
- Mbang Bonda BM, Etame J, Kouske AP, Bayiga EC, Ngon GF, Mbaï SJ, Gérard M (2017) Ore texture, mineralogy and whole rock geochemistry of the iron mineralization from Edea North Area, Nyong Complex, Southern Cameroon: implication for origin and enrichment process. *Int J Geosci* 8:659–677. <https://doi.org/10.4236/ijg.2017.85036>
- Montel JM, Foret S, Veschambre M, Nicollet C, Provost A (1996) A fast, reliable, inexpensive in-situ dating technique: electron microprobe ages of monazite. *Chem Geol* 131:37–53
- Montel JM, Kornprobst J, Vielzeuf D (2000) Preservation of old U–Th–Pb ages in shielded monazite: example from the Beni Bousera Hercynian kinzigites (Morocco). *J Metamorph Geol* 18:335–342. <https://doi.org/10.1046/j.1525-1314.2000.00261.x>
- Montel JM, Devidal JL, Avignat D (2002) X-ray diffraction study of brabantite–monazite solid solutions. *Chem Geol* 191:89–104
- Moussango Ibohn AP, Njom B, Sep Nlomngan JP, Ntantoh S, Mbog Bassong, SP, Ekodeck GE (2022) Characterization and tectonic significance of the deformation in the northern edge of the Paleoproterozoic Nyong Complex and identification of the fault systems of the Sanaga fault and Edea (Cameroon, Central Africa). *AJGS* 15(6). <https://doi.org/10.1007/s12517-022-09588-0>
- Mvodo H, Ganno S, Kouankap Nono GD, Fossi DH, Nga Essomba PE, Ma NT, Nzenti JP (2022) Petrogenesis, LA-ICP-MS zircon U–Pb geochronology and geodynamic implications of the Kribi metavolcanic rocks, Nyong Group, Congo craton. *Acta Geochim.* <https://doi.org/10.1007/s11631-022-00533-2>

- Nagy G, Draganits E (1999) Occurrence and mineral-chemistry of monazite and rhabdophane in the Lower and? Middle Austroalpine tectonic units of the southern Sopron Hills (Austria). *Mitt Ges Geol Bergbaustud Österr* 42:21–36
- Ndema Mbongué JL (2016) Evolution tectono-metamorphique de la serie du Nyong à Edea et à Eseka. Thèse de doctorat Ph.D, Université de Yaoundé I
- Ndema Mbongué JL, Aroke EA (2020) Petrology and geochemical constraints on the origin of banded iron formation-hosted iron mineralization from the Paleoproterozoic Nyong Serie (Congo Craton, South Cameroon), Pout Njouma Area (Edea North): Evidence for Iron Ore Deposits. *IJRIAS* 5(8):55–72
- Ndema Mbongué JL, Nzenti JP, Suh CE (2014) Origin and evolution of the formation of the Nyong serie in the Western Border of the Congo Craton. *J Geosci Geom* 2(2):62–75
- Ndema Mbongué JL, Sigué C, Nzenti JP, Suh CE (2019a) Structural characterization of outcrop-scale in Edea and Eseka area: evidence for a complex polyphase deformation in the Paleoproterozoic Nyong Serie (Congo craton-South Cameroon). *JAGG* 7(5):01–09
- Ndema Mbongué JL, Sigué C, Nzenti JP, Suh CE (2019b) Distribution of rare earth elements in the metamorphic rocks of the Paleoproterozoic Nyong Unit (Congo Craton, South – Cameroon). *J Appl Sci* 5(7):35–49
- Ngnotué T, Ganno S, Nzenti JP, Schulz B, Tchaptchet Tchato D, Suh Cheo E (2012) Geochemistry and geochronology of Peraluminous High-K granitic leucosomes of Yaoundé series (Cameroon): evidence for a unique Pan-African magmatism and melting event in North Equatorial Fold Belt. *Int J Geosci* 3:525–548
- Nsifa Nkonguin E, Tchameni R, Nédelec A, Siqueira R, Pouclet A, Bascou J (2013) Structure and petrology of Pan-African nepheline syenites from the South West Cameroon; implications for their emplacement mode, petrogenesis and geodynamic significance. *J Afr Earth Sc* 87:44–58
- Nzenti JP, Barbey P, Macaudiere J, Soba D (1988) Origin and evolution of the late Precambrian high-grade Yaounde gneisses (Cameroon). *Prec Res* 38:91–109
- Nzepang Tankwa M, Ganno S, Okunlola OA, Njiosseu T, Tamehe ELS, Woguia LK, Mbita MB, Nzenti JP (2021) Petrogenesis and tectonic setting of the Paleoproterozoic Kelle Bidjoka iron formations, Nyong group greenstone belts, southwestern Cameroon. Constraints from petrology, geochemistry, and LA-ICP-MS zircon U-Pb geochronology. *Int Geol Rev* 63(14):1737–1757
- Overstreet WC (1967) The geology occurrence of monazite. USGS, Professional paper 530, pp 294
- Owona S, Ondoa JM, Ratschbacher L, Ndzana SPM, Tchoua FM, Ekodeck GE (2011) The geometry of the Archean, Paleo- and Neoproterozoic tectonics in the Southwest Cameroon. *Comptes Rendus Geosci* 343:312–322. <https://doi.org/10.1016/j.crte.2010.12.008>
- Owona S, Tichomirowa M, Ratschbacher L, Mvondo Ondoa J, Youmen D, Pfänder JA, Affaton P (2012) New igneous (zircon Pb/Pb) and metamorphic (Rb/Sr) ages in the Neoproterozoic Yaoundé Group (Cameroon, Central Africa): Consequences for the orogenic evolution north of The Congo Craton. *Int J of Earth Sci* 101(7):1689–1703
- Owona S, Ratschbacher L, Gulzar MA, Nsangou Ngapna M, Mvondo Ondoa J, Ekodeck GE (2020) New U-Pb zircon ages of Nyong Complex meta-plutonites: inferences on the Eburnean/Trans-Amazonian orogeny in SW Cameroon (Central Africa) *Geol J* 1–15 <https://doi.org/10.1002/gj.4022>
- Owona S, Ratschbacher L, Nsangou Ngapna M, Gulzar AM, Ondoa M, Ekodeck JGE (2021a) How diverse is the source? Age, provenance, reworking, and overprint of Precambrian meta-sedimentary rocks of West Gondwana, Cameroon, from zircon U-Pb geochronology. *Prec Res* 359:106220
- Owona S, Ratschbacher L, Nsangou Ngapna M, Gulzar AM, Ondoa M, Ekodeck JGE (2021b) Reply to comment on ““How diverse is the source? Age, provenance, reworking, and overprint of Precambrian meta-sedimentary rocks of West Gondwana, Cameroon, from zircon U-Pb geochronology” by Mvondo and Bineli Betsi””. *Prec Res* 366:106418
- Owona S, Schulz B, Minyem D, Ratschbacher L, Chako Tchamabe BC, Olinga JB, Mvondo Ondoa J, Ekodeck GE (2022) Eburnean/Trans-Amazonian orogeny in the Nyong complex of southwestern Cameroon: meta-basite geochemistry and metamorphic petrology. *J Afric Earth Sci*. <https://doi.org/10.1016/j.jafrearsci.2022.104515>
- Parrish RR (1990) U-Pb dating of monazite and its application to geological problems. *Can J Earth Sci* 27:1431–1450
- Peiffert C, Cuney M (1999) Hydrothermal synthesis of the complete solid solution between Monazite (LaPO₄) and Huttonite (ThSiO₄) at 780°C and 200 Mpa. *J Conf Abstract* 4:522
- Penaye J, Toteu SF, Tchameni R, Van Schmus WR, Tchakounté J, Ganwa A, Minyem D, Nsifa EN (2004) The 2,1Ga West Central African Belt in Cameroon: extension and evolution. *J Afr Earth Sc* 39:159–164
- Perumalsamy C, Bhadra S, Balakrishnan S (2016) Decoding evolutionary history of provenance from beach placer monazites: a case study from Kanyakumari coast, southwest India. *Chem Geol* 427:83–97
- Petrík I, Janák M, Klonowska I, Maika J, Froitzheim N, Yoshida K et al (2019) Monazite behaviour during metamorphic evolution of a diamondbearing gneiss: a case study from the Seve Nappe Complex, Scandinavian Caledonides. *J Petrol* 60:1773–1796
- Poitrasson F, Chenery S, Bland DJ (1996) Contrasted monazite hydrothermal alteration mechanisms and their geochemical implications. *Earth Planet Sci Lett* 145:79–96
- Poitrasson F, Chenery S, Shepherd TJ (2000) Electron microprobe and LA-ICP-MS study of monazite hydrothermal alteration: implications for U-Th–Pb geochronology and nuclear ceramics. *Geochim Cosmochim Acta* 64:3283–3297
- Pouclet A, Tchameni R, Mezger K, Vidal M, Nsifa EN, Shang C, Penaye J (2007) Archaean crustal accretion at the Northern border of Congo Craton (South Cameroon) The charnockite-TTG ling. *Bull Soc Géol De France* 178:331–342
- Pyle JM, Spear FS (2003) Four generations of accessory phase growth in low-pressure migmatites from SW New Hampshire. *Am Miner* 88:338–351
- Pyle JM, Spear FS, Rudnick RL, McDonough WF (2001) Monazite-xenotime-garnet equilibrium in metapelites and a new monazite-garnet thermometer. *J Petrol* 42:2083–2107
- Rupasinghe MS, Gocht W, Dissanayake CB (1983) The genesis of thorium-rich monazite placer deposits in Sri Lanka. *J Natn Sci Coun Sri Lanka* 11(1):99–110
- Sawka WN, Banfield JF, Chappell BW (1986) A weathering-related origin of widespread monazite in S-type granites. *Geochim Cosmochim Acta* 50:171–175
- Schultz B (2021) Monazite microstructures and their interpretation in petrochronology. *Frontiers in Earth Sci* 9:1–22
- Schulz B, Brätz H, Bombach K, Krenn E (2007a) In situ Th-Pb dating of monazite by 266 nm laser ablation and ICPMS with a single collector, and its control by EMP analysis. – *Z. Angew Geol* 35:377–392
- Schulz B, Krenn E, Finger F, Brätz H, Klemd R (2007b) Cadomian and Variscan metamorphic events in the Léon Domain (Armorican Massif, France): P-T data and EMP monazite dating. *Geol Soc Am Special Paper* 423–12:267–285
- Seydoux-Guillaume AM, Montel JM, Bingen B, de Parseval VP, Paquette JL et al (2012) Low-temperature alteration of monazite: fluid mediated coupled dissolution-precipitation, irradiation damage, and disturbance of the U/Pb and Th/Pb chronometers.

- Chem Geol 33:140–158. <https://doi.org/10.1016/j.chemgeo.2012.07.031>
- Shang CK, Satirb M, Siebel W, Taubald H, Nsifa EN, Westphal M, Reitter E (2001) Genesis of K-rich granitoids in the Sangmelima region, Ntem complex (Congo craton), Cameroon. *Terra Nostra* 5:60–63
- Shang CK, Satirb M, Siebel W, Nsifa NE, Taubald H, Liegeois JP, Tchoua FM (2004) TTG magmatism in the Congo craton; a view from major and trace element geochemistry, Rb-Sr and Sm-Nd systematics: case of the Sangmelima region, Ntem complex, Southern Cameroon. *J Afric Earth Sci* 40:61–79
- Shang CK, Liégeois JP, Satirb M, Nsifa FW, EN, (2010) Late Archaean high-K granite geochronology of the northern metacratonic margin of the Archaean Congo craton Southern Cameroon: evidence for Pb-loss due to non-metamorphic causes. *Gondwana Res* 475:1–19
- Siivola J, Schmid R (2007) List of mineral abbreviations. Recommendations by the IUGS Subcommittee on the Systematics of Metamorphic Rocks. Web version. Web version 01 February 2007. www.bgs.ac.uk/scmr/home.html. Accessed 31 Dec 2013
- Soh Tamehe L, Wei C, Ganno S, Rosière CA, Nzenti JP, Ebotehou CG, Lu G (2021) Depositional age and tectonic environment of the Gouap banded iron formations from the Nyong group, SW Cameroon: Insights from isotopic, geochemical and geochronological studies of drillcore samples. *Geosci Frontiers* 12:549–572
- Soh Tamehe L, Wei C, Ganno S, Rosière CA, Li H, Soares MB, Nzenti JP, Santos JOS, Bekker A (2022) Provenance of metasiliclastic rocks at the northwestern margin of the East Gabonian Block: Implications for deposition of BIFs and crustal evolution in southwestern Cameroon. *Prec Res*. <https://doi.org/10.1016/j.precamres.2022.106677>
- Spear FS, Pyle JM (2002) Apatite, monazite and xenotime in metamorphic rocks. – In: Kohn M, Rakovan J, Hughes JM (Eds.) *Phosphates — geochemical, geobiological and materials importance*. Rev Mineral Geochem. Mineral Soc Am, Washington DC, 48:293–335
- Takam T, Arima M, Kokonyangi J, Dunkley DJ, Nsifa EN (2009) Paleoarchaean charnockite in the Ntem Complex, Congo Craton, Cameroon: insights from SHRIMP zircon U-Pb ages. *J Mineral Petrol Sci* 104:1–11. <https://doi.org/10.2465/jmps.080624>
- Taylor SR, McLennan SM (1985) *The continental crust: its composition and evolution*. Blackwell Publishing, Oxford, UK, p 312
- Tchameni R, Mezger K, Nsifa NE, Pouclet A (2000) Neoproterozoic evolution in the Congo craton: evidence from K rich granitoids of the Ntem complex, Southern Cameroon. *J Afric Earth Sci* 30:133–147
- Tchameni R, Pouclet A, Mezger K, Nsifa NE, Vicat JP (2004) Monozircon and Sm-Nd whole rock ages from the Ebolowa greenstone belts: Evidence for the terranes older than 2.9 Ga in the Ntem Complex (Congo craton, South Cameroon). *J CA Sci* 4:213–224
- Tchameni R, Lerouge C, Penaye J, Cocherie A, Milesi JP, Toteu SF, Nsifa NE (2010) Mineralogical constraint for metamorphic conditions in a shear zone affecting the Archean Ngoulemakong tonalite, Congo craton (Southern Cameroon) and retentivity of U-Pb SHRIMP zircon dates. *J Afr Earth Sci* 58:67–80
- Thiéblemont D, Callec Y, Fernandez-Alonso M, Chène F (2018) A geological and isotopic framework of Precambrian Terrains in Western Central Africa: an introduction. In: Siegesmund S, Basei MAS, Oyhantçal P, Oriolo S (eds) *Geology of South-west Gondwana*. Springer International Publishing, Cham, pp 107–132. https://doi.org/10.1007/978-3-319-68920-3_5
- Toteu SF, Van Schmus WR, Penaye J, Nyobe JB (1994) U-Pb and Sm-Nd evidence for Eburnian and Pan-African high grade metamorphism in cratonic rocks of southern Cameroon. *Precamb Res* 67:321–347
- Toteu SF, Van Schmus WR, Penaye J, Michard A (2001) New U-Pb and Sm-Nd data from North-Central Cameroon and its bearing on the pre-pan African history of Central Africa. *Prec Res* 108:45–73
- Toteu SF, Penaye J, Deloule E, Van Schmus WR, Tchameni R (2006) Diachronous evolution of volcano-sedimentary basins north of the Congo Craton: insights from U/Pb ion microprobe dating of zircons from the Poli, Lom and Yaoundé Groups (Cameroon). *J Afric Earth Sci* 44:428–442
- Townsend KJ, Miller CF, D'Andrea JL, Ayers JC, Harrison TM, Coath CD (2000) Low temperature replacement of monazite in the Ireteba granite, Southern Nevada: geochronological implications. *Chem Geol* 172:95–112
- Van Emden B, Thornber MR, Graham J, Lincoln FJ (1997) The incorporation of actinides in monazite and xenotime from placer deposits in Western Australia. *Canad Mineral* 35:95–104
- Williams ML, Jercinovic MJ (2002) Microprobe monazite geochronology: putting absolute time into microstructural analysis. *J Struct Geol* 24:1013–1028
- Wu L-G, Li X-H, Ling X-X, Yang Y-H, Li C-F, Li Y-L, Mao Q, Li Q-L, Putlitz B (2019) Further characterization of the RW-1 monazite: a new working reference material for oxygen and neodymium isotopic microanalysis. *Minerals* 9:583. <https://doi.org/10.3390/min9100583>
- Zhu XK, O'Nions RK (1999) Zonation of monazite in metamorphic rocks and its implications for high temperature thermochronology; a case study from the Lewisian terrain. *Earth Planet Sci Lett* 171:209–220

Springer Nature or its licensor (e.g. a society or other partner) holds exclusive rights to this article under a publishing agreement with the author(s) or other rightsholder(s); author self-archiving of the accepted manuscript version of this article is solely governed by the terms of such publishing agreement and applicable law.